OPEN ACCESS
CellPress

Cell Reports
Article

MicroRNA-Mediated Regulation of Dp53 in the *Drosophila* Fat Body Contributes to Metabolic Adaptation to Nutrient Deprivation

Lara Barrio,[1,3] Andrés Dekanty,[1,3,4] and Marco Milán[1,2,*]
[1]Institute for Research in Biomedicine (IRB Barcelona), Baldiri i Reixac, 10, 08028 Barcelona, Spain
[2]Institucio Catalana de Recerca i Estudis Avançats (ICREA), 08028 Barcelona, Spain
[3]Co-first author
[4]Present address: Instituto de Agrobiotecnología del Litoral (CONICET-UNL), 3000 Santa Fe, Argentina
*Correspondence: marco.milan@irbbarcelona.org
http://dx.doi.org/10.1016/j.celrep.2014.06.020
This is an open access article under the CC BY-NC-ND license (http://creativecommons.org/licenses/by-nc-nd/3.0/).

SUMMARY

Multiple conserved mechanisms sense nutritional conditions and coordinate metabolic changes in the whole organism. We unravel a role for the *Drosophila* homolog of p53 (Dp53) in the fat body (FB; a functional analog of vertebrate adipose and hepatic tissues) in starvation adaptation. Under nutrient deprivation, FB-specific depletion of Dp53 accelerates consumption of major energy stores and reduces survival rates of adult flies. We show that Dp53 is regulated by the microRNA (miRNA) machinery and *miR-305* in a nutrition-dependent manner. In well-fed animals, TOR signaling contributes to *miR-305*-mediated inhibition of Dp53. Nutrient deprivation reduces the levels of miRNA machinery components and leads to Dp53 derepression. Our results uncover an organism-wide role for Dp53 in nutrient sensing and metabolic adaptation and open up avenues toward understanding the molecular mechanisms underlying p53 activation under nutrient deprivation.

INTRODUCTION

The integration of nutrient status to metabolic homeostasis at the cellular and organismal level is a complex process performed in multicellular organisms, and the ability of an organism to respond to nutritional stress is critical for its survival. In the last few years, the tumor suppressor protein p53 has emerged as a key regulator of metabolic homeostasis that triggers a cellular adaptive response to fluctuations in nutrient availability (Berkers et al., 2013; Vousden and Ryan, 2009), a function that may contribute not only to tumor suppression activities of this molecule but also to its non-cancer-associated functions. Whereas p53 plays a major tumor suppressor role by inhibiting glycolysis and glutaminolsysis at different levels, thus suppressing glucose and glutamine flux into subsidiary pathways for biosynthesis in highly proliferative and growing tumor cells (Jiang et al., 2013), p53 induces metabolic remodelling and promotes cell survival upon transient metabolic stresses (Berkers et al., 2013). In cultured cells, p53 induces cell-cycle arrest and promotes cell survival in response to transient glucose deprivation (Jones et al., 2005), regulates autophagic flux and increases cell fitness upon starvation (Scherz-Shouval et al., 2010), and preserves the antioxidant capacity of the cell and increases survival rates upon serine deprivation (Maddocks et al., 2013).

Studies on the potential role of p53 in nutrient sensing and metabolic adaptation at the organismal level can benefit from genetically tractable model systems. In this regard, *Drosophila* is a highly attractive model system, where the fat body (FB), a functional analog of vertebrate adipose and hepatic tissues, functions as a key sensor that couples nutrient status and energy expenditure (Arrese and Soulages, 2010; Canavoso et al., 2001). In conditions of nutrient deprivation, the FB supplies energy to the rest of the body by mobilizing stored glycogen and triacylglycerides (TAGs) to circulation in the form of trehalose and diacylglycerides (DAGs), respectively (Arrese and Soulages, 2010). The *Drosophila* homolog of p53 (Dp53) shares significant amino acid identity with mammalian p53, including specific residues frequently associated with human cancer (Brodsky et al., 2000; Jin et al., 2000; Mandal et al., 2005, 2010; Ollmann et al., 2000). Like its mammalian counterparts, Dp53 promotes apoptotic cell death and cell-cycle arrest in response to several stresses, including DNA damage and mitochondrial dysfunction (Brodsky et al., 2000; Jin et al., 2000; Mandal et al., 2005, 2010; Ollmann et al., 2000).

Here, we have identified that Dp53 participates in organismal adaptation to nutrient deprivation. The depletion of Dp53 activity levels specifically in FB cells accelerates the consumption of the main energy stores, reduces the levels of sugars in the animal, and compromises organismal survival upon fasting. We present evidence that the levels of fasting hormones and metabolic enzymes that mobilize these energy resources are similarly modulated by starvation in control and *dp53* mutant animals and unveil a cell-autonomous role of Dp53 in modulating the metabolic changes of FB cells to nutrient deprivation. We also identified the molecular mechanism by which Dp53 is activated by nutrient conditions in FB cells. We present evidence that microRNAs (miRNAs), an abundant class of endogenous noncoding RNAs measuring 22–23 nt in length (Huntzinger and Izaurralde, 2011),

regulate *dp53* expression by targeting its 3′ UTR, and we identify *miR-305* as a major regulatory element. Interestingly, two elements involved in the biogenesis of miRNAs, Drosha and Dicer, and one catalytic component of the RNA-induced silencing complex (RISC), Argonaute-1, are downregulated during starvation, thus alleviating *miR-305*-dependent targeting of the *dp53-3′UTR* and contributing to organismal resistance to starvation. These results open up avenues toward the molecular understanding of p53 activation under metabolic stress and reveal the participation of p53 in nutrient sensing and metabolic adaptation at the organismal level.

RESULTS

Dp53 Plays an FB-Specific Role in Regulating Energy Metabolism under Nutrient Deprivation

To study whether Dp53 is involved in nutrient sensing and metabolic adaptation at the organismal level, we exposed young adult flies (1 to 2 days old) to acute starvation (2% agar, 1% sucrose; Géminard et al., 2009) and compared the survival rates of *dp53* mutant and control animals. Two null alleles of *dp53* (*dp53^{ns}* and *dp53^{5A14}*), backcrossed six times into the *w^{1118}* genetic background, were used. Loss of Dp53 activity produces phenotypically wild-type adult flies and induces a lifespan extension under normal food conditions (Bauer and Helfand, 2009; Waskar et al., 2009). Under nutrient deprivation, however, a clear reduction in the survival rates of *dp53* mutant adult flies was observed when compared to controls (Figures 1A–1D; Table S1). Reduced survival rates were observed in both males and females and also in 5- to 7-day-old adult flies subjected to starvation (Figure S1; Table S1). Similar effects on survival rates were obtained in young adult flies or larvae exposed to complete nutrient deprivation (2% agar, 0% sucrose in the case of adults, and PBS-soaked paper in the case of larvae), as well as in larvae exposed to diluted (0,2X) food (Figure S1; Table S1). In the latter case, survival rates were measured as the percent of individuals entering pupariation or giving rise to adult flies (Figure S1). Flies store energy mainly as TAGs and glycogen (Arrese and Soulages, 2010), and these reserves are used under nutrient deprivation. While TAG and glycogen levels were not significantly different in *dp53* mutant and control animals at the beginning of the starvation procedure (Figure S1), they were used at higher rates in fasted *dp53*-depleted animals (Figures 1E and 1F). These results indicate that *dp53* mutant flies deplete their energetic reserves faster, which might contribute to their poor survival rates in fasting conditions.

The molecular mechanisms by which vertebrates and flies regulate the storage and release of fuel molecules at the systemic level display significant parallels. The adipokinetic hormone (AKH), the functional analog of the vertebrate glucagon, plays a key role in mobilizing energy resources during fasting, whereas *Drosophila* insulin-like peptides (dILPs) promote energy storage in normal feeding conditions, recapitulating the role of the vertebrate insulin pathway (Bharucha et al., 2008; Kim and Rulifson, 2004; Rulifson et al., 2002). Brain insulin-producing cells (IPCs) secrete dILPs in response to nutrition and accumulate dILPs under nutrient deprivation (Géminard et al., 2009). Despite the accelerated consumption of energy resources observed in starved *dp53* mutant animals when compared to control individuals, AKH production was increased, in a similar manner, in both genotypes upon fasting (Figure 1G; see also Figure S1). Insulin signaling (measured as an increase in the levels of the *Drosophila* insulin receptor, *dInR*, and *4EBP*) was also similarly reduced in both genotypes upon fasting (Figures 1H and 1I). *4EBP* and *dInR* are two targets of dFOXO transcription factor (Puig et al., 2003; Teleman et al., 2005), which is negatively regulated by the insulin pathway. Thus, an increase in the levels of these two genes reflects a reduction in insulin signaling. Consistent with this, dILP2 protein was similarly accumulated in IPCs of both control and *dp53* mutant animals upon fasting (Figures 1J and 1K). Altogether, these results indicate that Dp53 has an impact on energy balance upon fasting that cannot be explained merely by a failure in the regulation of dILPs and AKH production, thus suggesting a tissue-specific role of Dp53.

The FB of insects functions as a key sensor to couple nutrient status and energy expenditure and serves as a repository for both TAGs and glycogen, combining the energy storage functions of vertebrate adipose and hepatic tissues, respectively (Arrese and Soulages, 2010; Canavoso et al., 2001). We then analyzed whether Dp53 plays a role in this key organ during starvation. We specifically reduced Dp53 activity in the FB using the Gal4/upstream activating sequence (UAS) system (Brand and Perrimon, 1993) and determined survival rates as well as the consumption of energy reserves upon fasting. We used two transgenes (*UAS-dp53$^{H159.N}$*, a dominant-negative version of Dp53 carrying a point mutation in the DNA binding domain [Ollmann et al., 2000], and *UAS-dp53^{RNAi}*, a double-stranded RNA [dsRNA] form of *dp53*) and three GAL4 drivers expressed in the adult FB (*ppl-GAL4*, *cg-GAL4*, and *yolk-GAL4*) to deplete Dp53 activity in this key organ. In all cases, depletion of Dp53 activity in the FB reduced survival rates upon fasting (Figures 2A–2D and 2F; Table S1) when compared to control flies expressing GFP under the same drivers in the FB. Similar effects on survival rates were obtained in flies exposed to complete nutrient deprivation (2% agar, 0% sucrose; Figure S2; Table S1). Parental UAS lines alone (*UAS-dp53$^{H159.N}$* and *UAS-dp53^{RNAi}*) showed similar survival rates upon fasting than control UAS-GFP flies (Figure S2; Table S1). Interestingly, muscle-specific depletion of Dp53 activity (using the *mef2-gal4* driver; Demontis and Perrimon, 2010; Ranganayakulu et al., 1995) did not have any impact on the survival rates upon fasting (Figure 2E; Table S1). In accordance with the reduced viability upon fasting caused by targeted reduction of Dp53 in FB cells, TAGs and glycogen were consumed at accelerated rates in these animals (Figures 2I and 2J) and the levels of sugars in the animal were further reduced when compared to control individuals (Figure 2K). Remarkably, and consistent with the fact that the starvation-induced reduction in dILP secretion and the increase in Akh transcription, hormones involved in the tight regulation of sugars in circulation, were unaffected by Dp53 depletion (Figures 1G–1K), the levels of circulating sugars were similarly reduced upon fasting in wild-type and Dp53-depleted animals (Figure 2L). Thus, FB-specific depletion of Dp53 causes an accelerated consumption of energy resources. The levels of TAGs, glycogen, and sugars were largely similar in *dp53*-depleted and control animals at the beginning of the starvation procedure (Figure S2).

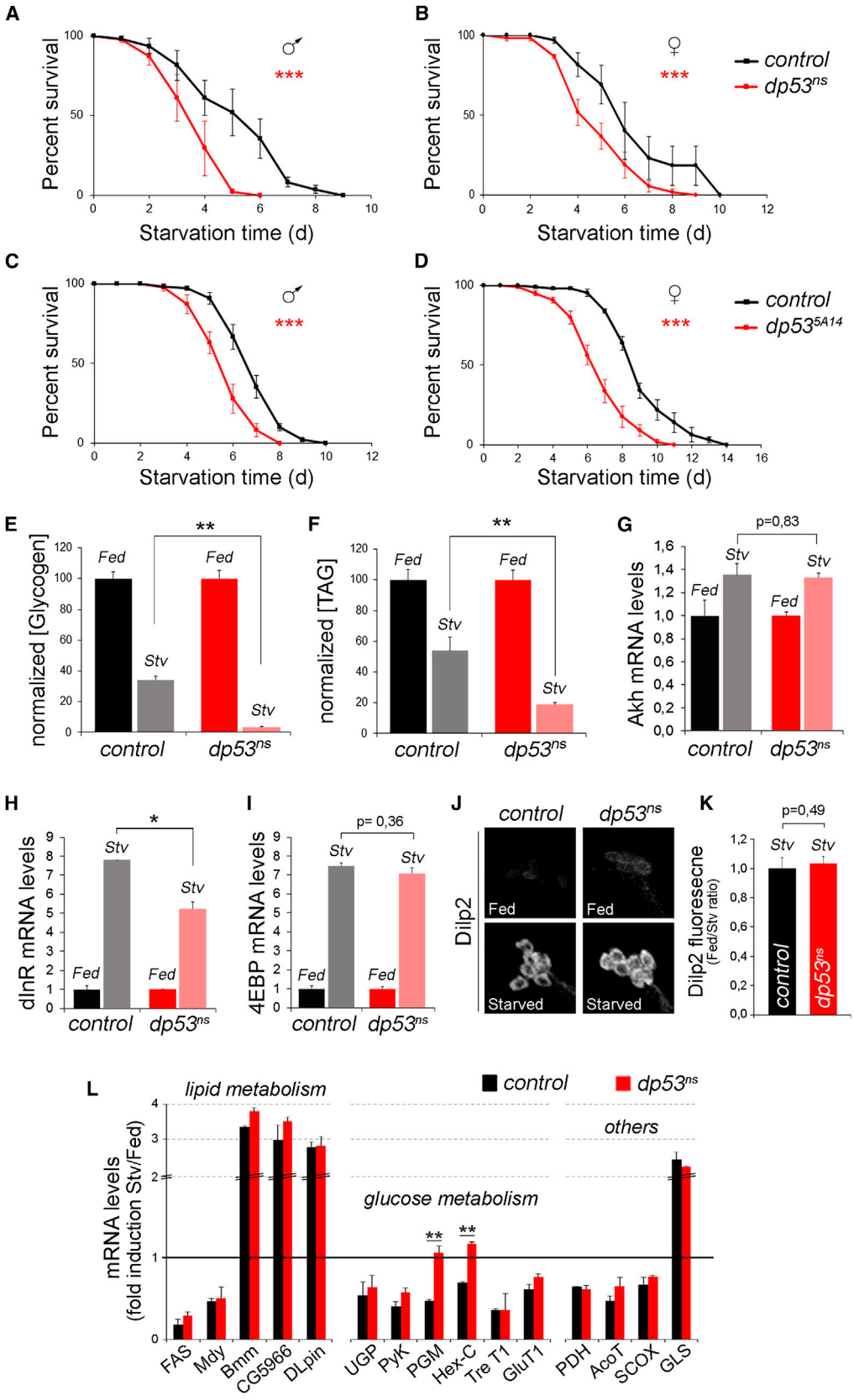

(legend on next page)

Intracellular TAG storage occurs in specialized cytoplasmic compartments called lipid droplets. In line with the accelerated TAG consumption observed in starved *dp53* mutant flies, specific depletion of Dp53 in single FB cells caused smaller lipid droplets (labeled by Nile red staining) than in wild-type cells upon fasting (Figure 2N). No significant change in lipid droplet size was observed in well-fed FB cells depleted for Dp53 activity (Figure 2M). Altogether, these results indicate that Dp53 plays a cell-autonomous and FB-specific role in metabolic adaptation to starvation, as energy store breakdown is accelerated in Dp53-depleted animals and survival rates are compromised. Consistent with this proposal, overexpression of Dp53 in FB cells increased the starvation resistance of adult flies (Figure 2G), and FB-specific expression of Dp53 rescued the reduced survival rates of starved *dp53* mutant animals (Figure 2H).

Since Dp53 activity modulates the levels of energy store breakdown and the amount of stored fat in individual cells, it is likely to operate via the regulation of cellular metabolism. We thus measured RNA levels, by quantitative RT-PCR, of a panel of 15 key metabolic enzymes in fed and starved individuals (Figure 1L). In conditions of nutrient deprivation, the FB supplies energy to the rest of the body by mobilizing stored resources to circulation (Arrese and Soulages, 2010). Consistently, a pronounced increase in the expression levels of the Brummer lipase (the homolog of the mammalian adipose triglyceride lipase; Grönke et al., 2005) and the CG5966 lipase, both used to mobilize stored TAGs in the FB (Kühnlein, 2012), and a clear reduction in the expression levels of lipogenic enzymes, such as fatty acid synthase and Midway, were observed in control animals upon fasting (Figure 1L). We also observed in these animals a drastic reduction in the expression levels of metabolic enzymes involved in glycolysis (pyruvate kinase, phosphoglucose mutase, and hexokinase C), cellular respiration (pyruvate dehydrogenase), and fatty acid oxidation (acetyl-coenzyme A thiolase and cytochrome *c* oxidase). These changes might reflect reduced rates of glucose and fatty acid catabolism in starved FB cells and a preferential use of these metabolites for the production of circulating sugars and lipids to be used by peripheral tissues during fasting periods.

Dp53 activity does not appear to directly modulate the levels of those enzymes involved in mobilizing energy resources during starvation (Figure 1L). *Drosophila* Lipin (dLpin), a central regulator of adipose tissue development that promotes survival to starvation (Ugrankar et al., 2011), was also similarly upregulated in control and *dp53* mutant flies. Interestingly, we noticed that the levels of the glycolytic enzymes phosphoglucose mutase (PGM) and hexokinase-C (HexC) remained unchanged in *dp53* mutant flies (Figure 1L). These differences suggest an active glycolytic pathway in starved *dp53* mutant flies, which is consistent with the reduced amount of sugars under nutrient deprivation (Figure 2K). This reduction might contribute to their poor survival rates, as an increase in the concentration of sugar in the medium (2% agar, 10% sucrose) rescued the survival rates of starved *dp53* mutant animals (Figure S1). These results point to a role of Dp53 in metabolic adaptation to nutrient deprivation of FB cells and suggest that reduced survival rates of fasted *dp53* mutant animals are most probably a consequence of deregulated consumption of sugar and faster depletion of energy resources.

Dp53 Is a Target of the miRNA Machinery

p53 is tightly regulated and maintained at low physiological levels in unstressed cells to prevent its deleterious effects on living organisms. We then examined whether Dp53 is specifically activated upon starvation in FB cells. For this purpose, we used a reporter of Dp53 activity that places a nuclear GFP (GFPnls) under the control of an enhancer of the *reaper* (rpr) locus that includes a p53 consensus binding site (*dp53R-GFPnls*; Lu et al., 2010). This reporter has been used in different cellular contexts to monitor induction of Dp53 activity upon several stresses. As shown in Figures 2O and 2P, Dp53 activity levels were increased in FB cells subjected to starvation as monitored by the rise in nuclear GFP expression levels of starved *dp53R-GFPnls* animals.

In mammals, a complex array of posttranslational modifications negatively regulates the stability, localization, conformation, and transcriptional activity of p53 in healthy cells (Gu and Zhu, 2012). Although the most critical step is the regulation of p53 by ubiquitin ligases such as Mdm2 (Toledo and Wahl, 2006), recent studies confirmed the old hypothesis that *Drosophila* lacks Mdm2 (Lane and Verma, 2012). In the last few years, the expression and activity of vertebrate p53 has been shown to be under the control of miRNAs (Hermeking, 2012). In order to address the contribution of the miRNA machinery to regulating Dp53 levels, we constructed a transgene consisting of the 3′ UTR of *dp53*, which is shared by the three alternative spliced forms, cloned into a tubulin-promoter-EGFP reporter plasmid (*dp53-sensor*; Figure 3A). The contribution of the miRNA machinery to regulating Dp53 levels was tested by depleting Dcr-1 activity, a critical element for miRNA biogenesis (Lee

Figure 1. Dp53 Modulates the Consumption of the Main Energy Storages upon Fasting and Contributes to Animal Resistance to Starvation

(A–D) Survival rates to nutrient deprivation of *dp53* mutant ($dp53^{ns}$ in A and B and $dp53^{5A14}$ in C and D) and control (w^{1118}) flies. Both males (A and C) and females (B and D) are shown. See Table S1 for n, p, median, and maximum survival values. The p value tests the null hypothesis that the survival curves are identical.

(E and F) Histograms plotting glycogen (E) and TAG (F) levels from adult male *dp53* mutant ($dp53^{ns}$) and control (w^{1118}) flies under fed or starved (Stv) conditions. Data were normalized to protein concentration and presented as a percentage of the fed values for each genotype.

(G–I) Histograms plotting Akh (G), dInR (H), and 4EBP (I) mRNA levels from adult male *dp53* mutant ($dp53^{ns}$) and control (w^{1118}) flies subjected to fed or starved (Stv) conditions. Results are expressed as fold induction with respect to fed conditions for each genotype. Heads were used in (G) and full bodies in (H) and (I).

(J) Brain IPCs stained to visualize dILP2 (white) protein levels in *dp53* mutant ($dp53^{ns}$) and control (w^{1118}) animals under fed or starved conditions.

(K) Histogram plotting mean dILP2 fluorescence intensity as a Fed/Stv ratio of IPCs shown in (I). Results were normalized to control flies.

(L) Histograms plotting mRNA levels of a collection of 15 key metabolic enzymes from adult males of *dp53* mutant ($dp53^{ns}$) and control (w^{1118}) flies subjected to fed or starved (Stv) conditions. Results are expressed as fold induction with respect to fed conditions for each genotype.

Animals were starved on 2% agar, 1% sucrose chronically (A–D), for 24 hr (E and G–L), or for 72 hr (F).

Error bars represent SEM. ***$p < 0.001$, **$p < 0.01$, and *$p < 0.05$.

See also Figure S1 and Tables S1 and S2.

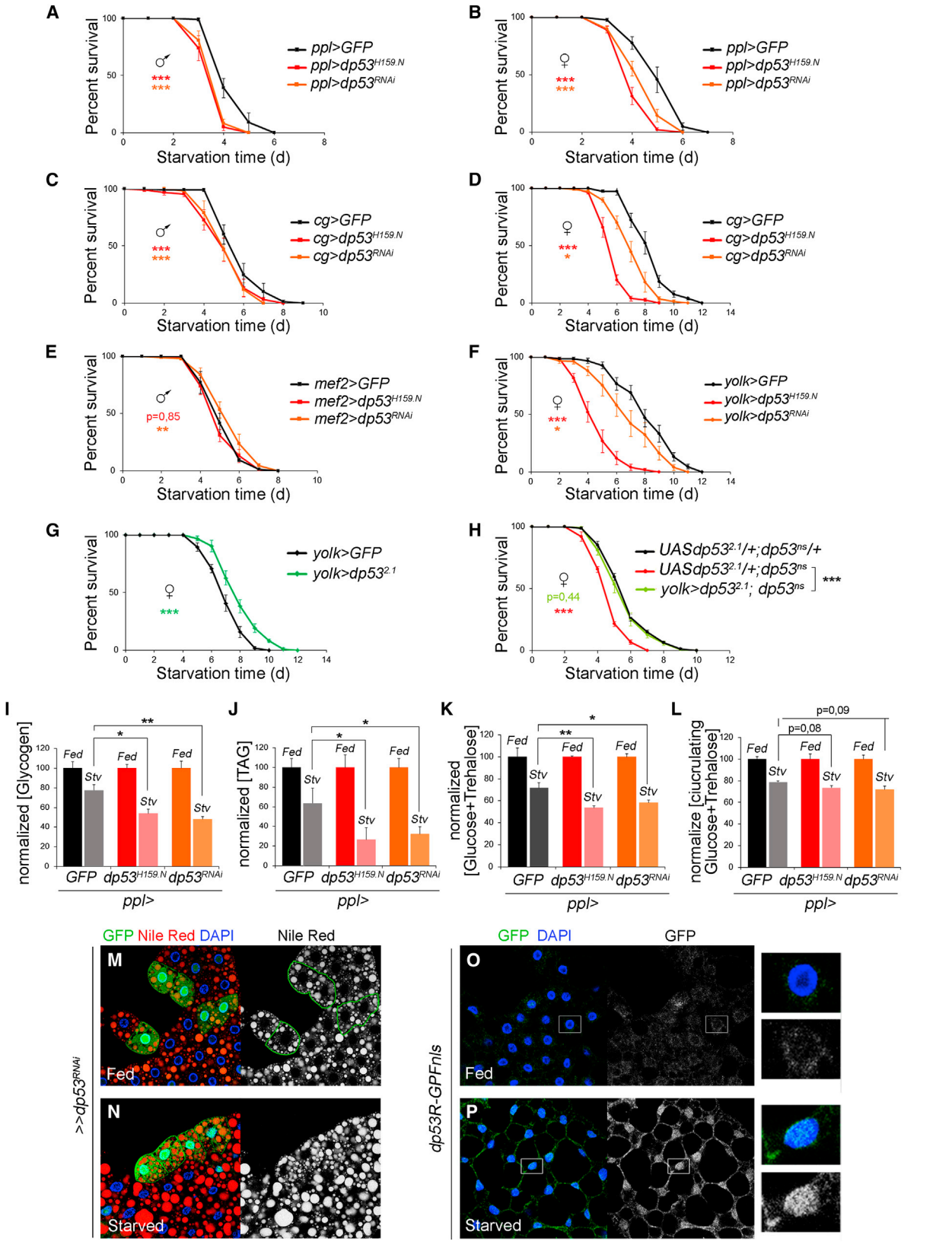

(legend on next page)

et al., 2003). miRNA-mediated targeting of the *dp53 3′UTR* is expected to maintain enhanced GFP (EGFP) expression levels of the *dp53 sensor* low under normal physiological conditions (Figures 3B and 3G). We first used the larval wing primordium, a simple epithelium, to address the contribution of the miRNA machinery to targeting the *dp53-sensor*. Expression of a dsRNA form of *dcr-1* (*dcr-1*^{RNAi}) either with ubiquitous (*actin*-Gal4; Figure S3) or region-specific (*hh*-Gal4 and *ptc*-Gal4; Figures 3C and S3) Gal4 drivers induced an increase in EGFP levels of the *dp53-sensor* in wing cells. Clones of cells mutant for a null allele of *dcr-1* (*dcr-1*^{Q1147X}; marked by the absence of β-galactosidase [β-gal]) also showed increased EGFP expression levels of the *dp53-sensor* when compared to the surrounding heterozygous tissue (Figure 3D, red arrows).

To further characterize the regulation of *dp53* by the miRNA machinery, we searched for potential miRNA binding sites in its 3′ UTR. Ten putative miRNAs were predicted to target the 3′ UTR of *dp53* (Figure S3). We assessed the capacity of these miRNAs to reduce the activity of a *dp53* 3′ UTR luciferase reporter in S2 cells and the EGFP expression levels of the *dp53-sensor* in wing disc cells. Five miRNAs reduced the activity of the *dp53* 3′ UTR luciferase reporter when overexpressed in S2 cells (Figure S3), and only three of these five (*miR-219*, *miR-283*, and *miR-305*) reduced the *dp53-sensor* in wing disc cells (Figures 3H and S3). Interestingly, the predicted binding site for *miR-305* targeted *dp53* in a region that is conserved among *Drosophila* species (Figure S3). In addition, *miR-305* showed high expression values in a large-scale sequencing of small RNAs in *Drosophila*, while miR-219 and miR-283 were underrepresented (Ruby et al., 2007). Using quantitative RT-PCR, we confirmed that *miR-305* was indeed highly enriched in FB cells (data not shown). These results support the proposal that *miR-305* is a biologically relevant candidate miRNA involved in regulating Dp53 levels in *Drosophila* tissues. To further characterize the role of *miR-305* in regulating *dp53*, we generated an EGFP sensor carrying the *dp53 3′UTR* lacking the predicted *miR-305* binding site (*dp53Δ305-sensor*; Figures 3E and 3F). *miR-305* overexpression did not reduce the EGFP levels of the *dp53Δ305-sensor* (compare Figures 3H and 3J), thereby indicating that regulation of the *dp53 3′UTR* by this miRNA depends on the presence of the predicted *miR-305* binding site. We observed that the EGFP expression levels of the *dp53Δ305-sensor* were consistently higher than those in the *dp53-sensor* carrying the whole 3′ UTR (compare Figures 3G and 3I). This finding thus suggests that *miR-305* has an active role in targeting *dp53 3′UTR* under normal physiological conditions. Consistent with this proposal, clones of cells (marked by the absence of β-gal) homozygous for a small deficiency covering the *miR-305* locus (*Df-miR-305*, for details see the Experimental Procedures) showed increased EGFP levels of the *dp53-sensor* (Figure 3K, red arrows). The resulting *wild-type* twin clones (marked by two copies of β-gal) showed reduced levels of the *dp53-sensor* (Figure 3K, yellow arrows) when compared to the surrounding heterozygous tissue. Thus, regulation of the *dp53-3′UTR* appears to be highly sensitive to the doses of *miR-305*. Interestingly, no apparent differences in the *dp53Δ305-sensor* were observed in clones of cells lacking *miR-305* (Figure 3L, red arrows). These results indicate that *miR-305* contributes to the regulation of *dp53* and that this regulation depends on the presence of the predicted *miR-305* binding site. We found that the increase in EGFP expression levels caused by *miR-305* depletion was milder than that observed in clones of cells mutant for *dcr-1* (compare Figures 3D and 3K). Thus, other miRNAs might contribute to regulating Dp53 levels in the wing disc. Consistently, clones of cells mutant for a null allele of *dcr-1* showed increased EGFP expression levels of the *dp53Δ305-sensor* (Figure S3).

Regulation of Dp53 by *miR-305* Is Modulated by Nutritional Conditions

We next addressed whether the regulation of *dp53* by the miRNA machinery also takes place in FB cells and whether this regulation is modulated by the nutritional status of the animal. Dp53 is indeed a target of the miRNA machinery in FB cells, as FB cells expressing *dcr-1*^{RNAi} showed increased EGFP levels of the *dp53-sensor* (Figure 4A; cells were marked by the absence of CD2) and FB cells expressing *miR-305* showed a reduction in the *dp53-sensor* EGFP levels (Figure 4B; cells were marked by the expression of red fluorescent protein). In order to address the potential modulation of this regulation by nutritional status, the EGFP levels of the *dp53-sensor* were analyzed in FB cells of starved and nonstarved animals. Although the EGFP

Figure 2. A FB-Specific Role of Dp53 in the Metabolic Adaptation to Nutrient Deprivation

(A–F) Survival rates to nutrient deprivation of adult flies expressing *GFP*, *Dp53*$^{H159.N}$, or *dp53*^{RNAi} in FB cells (A–D and F) or muscle cells (E) under the control of the *ppl-gal4* (A and B), *cg-gal4* (C and D), *mef2-gal4* (E), and *yolk-gal4* (F) drivers. Both males (A, C, and E) and females (B, D, and F) are shown. *yolk-GAL4* is expressed only in females.

(G) Survival rates to nutrient deprivation of adult females expressing *GFP* or a wild-type form of Dp53 (Dp53$^{2.1}$) under the control of the *yolk-gal4* driver.

(H) Survival rates to nutrient deprivation of adult females of the indicated genotypes. Note rescue in the survival rates to starvation of *dp53*^{ns} mutant flies upon expression of Dp53$^{2.1}$ in the FB.

See Table S1 for n, p, median, and maximum survival values. The p value tests the null hypothesis that the survival curves are identical.

(I–L) Histograms plotting whole-body glycogen (I), TAG (J), total glucose plus trehalose (K), or hemolymph glucose plus trehalose (L) levels from adult flies expressing *GFP*, *Dp53*$^{H159.N}$, or *dp53*^{RNAi} in FB cells under fed or starved (Stv) conditions. Data were normalized to protein concentration and presented as a percent of the fed values for each genotype.

Animals were starved on 2% agar, 1% sucrose chronically (A–H), for 24 hr (I, K, and L), or for 72 hr (J). Error bars represent SEM. ***$p < 0.001$; **$p < 0.01$, and *$p < 0.05$.

(M and N) Lipid droplets, visualized by Nile red staining (in red or white), in FB cells of fed (M) and starved (N) animals. Starved FB cells expressing *dp53*^{RNAi} (marked by the expression of GFP, in green) showed smaller lipid droplets that the neighboring wild-type cells. DAPI (in blue) labels FB nuclei.

(O and P) FB cells labeled to visualize the GFP levels (in green or white) of a Dp53 activity reporter construct (*dp53R-GFPnls*) in fed (O) or starved for 48 hr (P) animals.

See also Figure S2 and Table S1.

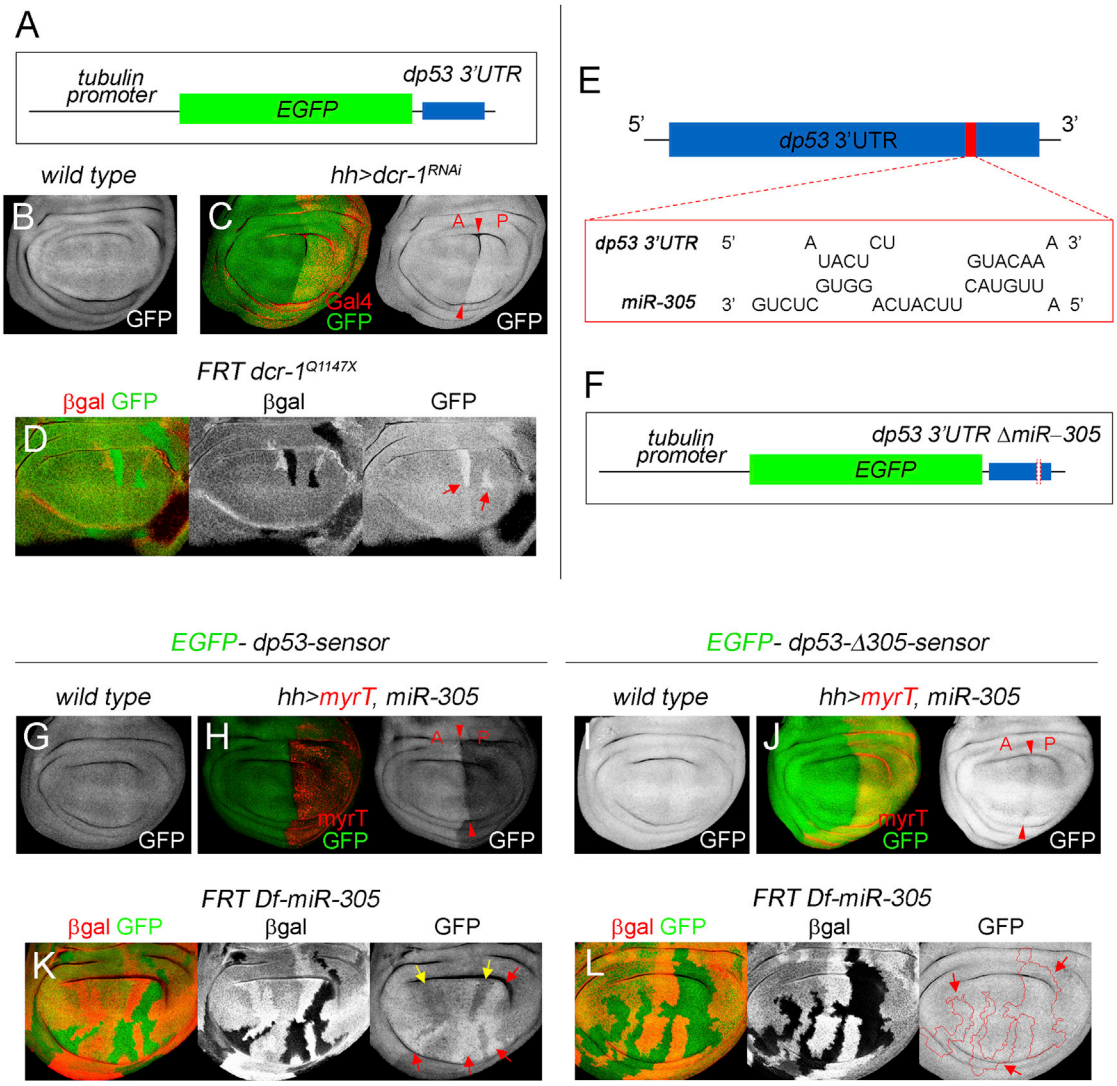

Figure 3. Dp53 Is a Target of *miR-305*

(A) Cartoon depicting the tubulin-EGFP transgene carrying the 3′ UTR of dp53 (*dp53-sensor*).

(B and C) Wing discs carrying the *dp53-sensor* and stained to visualize EGFP (green) and Gal4 (red) protein expression. The wing disc in (C) expressed *dcr-1*^{RNAi} under the control of the *hh-Gal4* driver. Red arrowheads depict the anterior-posterior (A-P) boundary.

(D) *dcr-1*^{Q1147X} homozygous clones (marked by the absence of *β-gal*, in red) showing expression of the *dp53-sensor* (green). Note increased levels of EGFP in *dcr-1*-depleted cells (red arrows).

(E) Representation of the putative binding site of *miR-305* in the *3′UTR* of *dp53*.

(F) Cartoon depicting the tubulin-EGFP transgene carrying the *3′UTR* of *dp53* with a deletion covering the *miR-305* seed region (*dp53Δ305-sensor*).

(G–J) Wing discs carrying the *dp53-sensor* (G and H) or the *dp53Δ305-sensor* (I and J) and stained to visualize EGFP (green) protein expression. Wing discs in (H) and (J) overexpressed *miR-305* and myrTomato (myrT) under the control of the *hh-Gal4* driver. Note reduced levels of the *dp53-sensor*, but not the *dp53Δ305-sensor*, in *miR-305*-overexpressing cells. Red arrowheads depict the A-P boundary.

(K and L) *Df(miR-305)* homozygous clones (marked by the absence of *β-gal* in red) showing expression of the *dp53-sensor* (K) or *dp53Δ305-sensor* (L). Note increased levels of the *dp53-sensor*, but not the *dp53Δ305-sensor*, in *Df(miR-305)* cells (red arrows). Also note in (K) decreased EGFP levels in twin clones with two wild-type copies of *miR-305* (yellow arrows).

See also Figure S3.

levels of a control sensor (Brennecke et al., 2003) were mildly reduced upon starvation, most probably as a consequence of the decrease in whole-animal metabolism (Figures 4C and 4C′; quantification in Figure 4F), the *dp53-sensor* was expressed at higher levels in starved than in normally fed individuals (Figures 4D and 4D′; quantification in Figure 4F). Remarkably, the impact of nutritional conditions on the *dp53-sensor* depended on the presence of the *miR-305* binding site, as no significant changes in the EGFP levels were observed in FB cells carrying the *dp53Δ305-sensor* and subjected to starvation (Figures 4E and

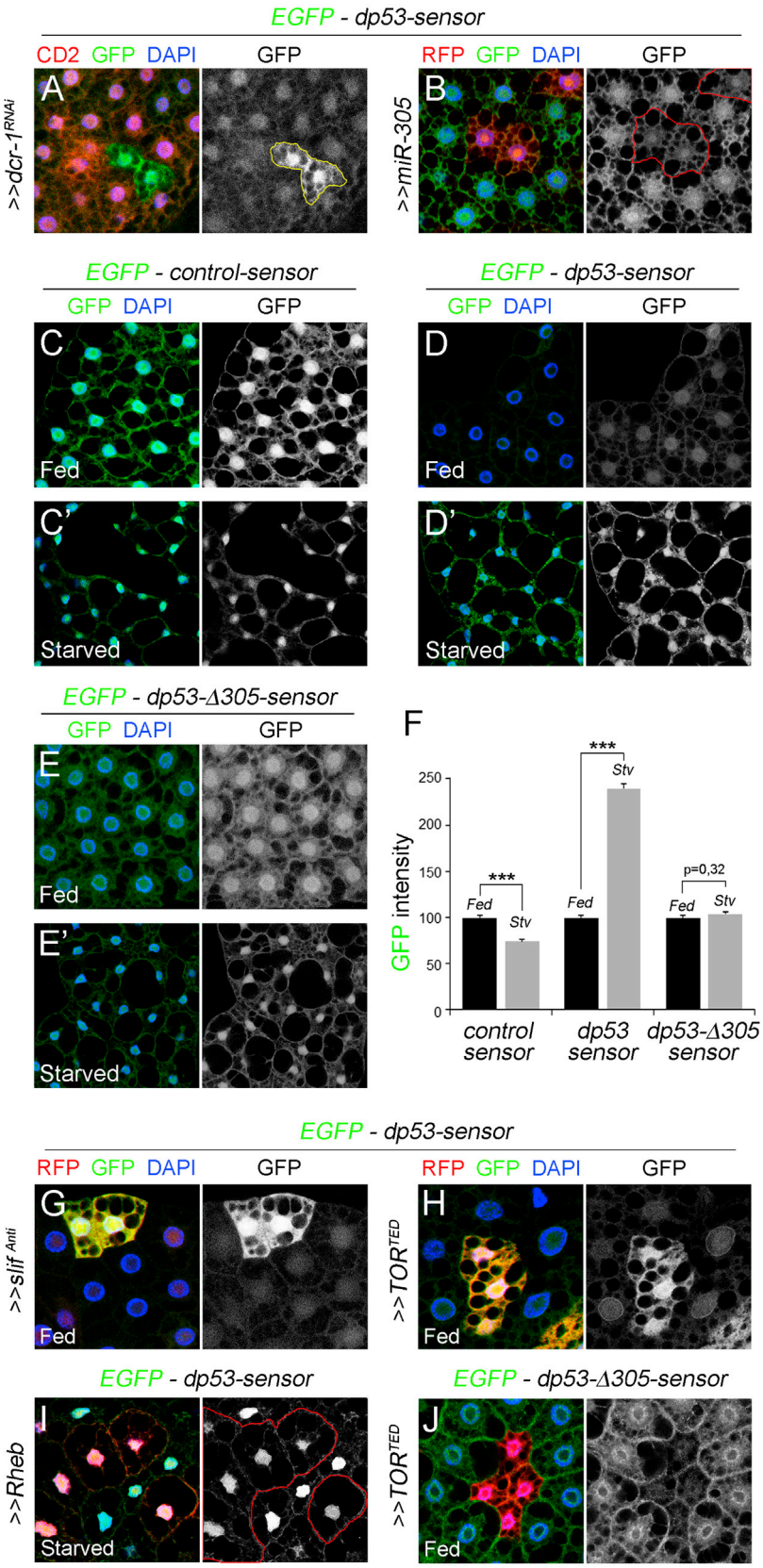

Figure 4. *miR-305*-Dependent Regulation of Dp53 Is Modulated by Nutrition

(A and B) FB cells of well-fed animals expressing *dcr-1*^{RNAi} (marked by the absence of CD2) or overexpressing *miR-305* and red fluorescent protein (RFP) (red), carrying the *dp53-sensor*, and stained to visualize EGFP (green) and CD2 (red) protein expression. Note increased EGFP levels in *dcr-1*^{RNAi} expressing cells and reduced EGFP levels upon *miR-305* overexpression.

(C–E) EGFP levels of the control sensor (C and C′), *dp53-sensor* (D and D′), or *dp53Δ305-sensor* (E and E′) in the FB of animals fed (C, D, and E) or starved for 48 hr (C′, D′, and E′).

(F) Histogram plotting EGFP expression levels of FB cells shown in (C)–(E). Results are normalized to the fed condition for each genotype. Note increased levels of *the dp53-sensor*, but not of the *dp53Δ305-sensor* and control sensor, under starvation. Error bars represent SEM. ***$p < 0.001$.

(G, H, and J) FB cells expressing RFP (red) and slif^{Anti} (G) or TOR^{TED} (H and J) in well-fed animals carrying the *dp53-sensor* (G and H) or the *dp53Δ305-sensor* (J) and stained to visualize EGFP (green) protein expression.

(I) FB cells expressing RFP and Rheb in starved animals carrying the *dp53-sensor* and stained to visualize EGFP (green) protein expression. Note increased EGFP levels in starved FB cells and reduced levels upon Rheb overexpression (enlarged cells delimited by red lines).

4E′; quantification in Figure 4F). These results support a major contribution of *miR-305* in targeting Dp53 in FB cells and imply that the regulation of the *dp53 3′UTR* is modulated by the nutritional status of the animal.

The major nutritional signal sensed by FB cells is amino acid availability, and downregulation of the amino acid transporter Slimfast (Slif) in the FB phenocopies amino acid deprivation (Colombani et al., 2003). TOR, an essential regulator of cell and tissue growth, is regulated in response to amino acid availability (Grewal, 2009; Hietakangas and Cohen, 2009). Once activated, TOR signaling modulates a variety of cellular processes such as protein synthesis, ribosome biogenesis, and autophagy. Thus, TOR signaling functions as the main nutritional sensor of a cell by coupling nutrient status to metabolic activity. We then examined whether genetic modulation of Slif or TOR activities in FB cells modulates the EGFP levels of the *dp53-sensor*. Well-fed animals showed a clear increase in the EGFP expression levels of the *dp53-sensor* in FB cells expressing an RNA antisense form of slif ($slif^{Anti}$; Figure 4G) or a dominant-negative version of TOR (TOR^{TED}; Figure 4H; Hennig and Neufeld, 2002). In contrast, activation of TOR (by expressing the GTPase Rheb, a positive regulator of TOR complex 1) in otherwise starved animals is expected to genetically mimic feeding conditions. Consistently, Rheb overexpression in FB cells strongly reduced the capacity of nutrient deprivation to upregulate the EGFP expression levels of the *dp53-sensor* (Figure 4I). Taken together, these results indicate that modulation of the *dp53-sensor* in FB cells is a cell-autonomous process that depends on TOR activity and support the notion that Dp53 is activated in FB cells by nutrient deprivation. Interestingly, the impact of TOR on the *dp53-sensor* depended on the presence of the *miR-305* binding site, as no increase in the EGFP levels was observed in FB cells carrying the *dp53Δ305-sensor* and expressing TOR^{TED} (Figure 4J; compare with Figure 4H). On the contrary, GFP expression levels were mildly reduced, most probably due to the reduction in translation caused by the strong depletion of TOR activity in these cells. These results reinforce the proposal that TOR signaling affects Dp53 activity levels through *miR-305*.

Nutrition-Dependent Regulation of the miRNA Machinery Contributes to Starvation Resistance

Nutrient conditions modulate, through Slif and TOR signaling, the capacity of *miR-305* to target *dp53* via its 3′ UTR, thus raising the possibility that *miR-305* levels are directly regulated by nutritional status. In order to address this possibility, we subjected adult flies to starvation and determined the levels of *miR-305* and seven other miRNAs by quantitative RT-PCR. Remarkably, the levels of six miRNAs, including *miR-305*, were reduced upon starvation (Figure 5A), suggesting a general rather than specific downregulation of miRNAs upon starvation. Emerging data have provided evidence that the whole miRNA machinery can be targeted under several stress conditions (Blandino et al., 2012; Gibbings et al., 2012; Ho et al., 2012), thus opening up the possibility that the miRNA-processing machinery itself is targeted under nutrient deprivation in FB cells. Consistent with this proposal, the expression levels of Dicer-1 and Drosha, enzymes involved in miRNA processing, and Argonaute-1, a catalytic component of RISC (Huntzinger and Izaurralde, 2011), were reduced both in starved adult flies and starved larval FBs (Figures 5B and 5C). These results indicate that starvation reduces the expression levels of central elements of the miRNA machinery and, consequently, alleviates *miR305*-mediated targeting of the *dp53-sensor* in FB cells. Consistent with this proposal, overexpression of *miR-305* in FB cells of starved animals was unable to reduce the EGFP levels of the *dp53-sensor* (Figure 5D, red arrowheads), whereas it was able to do so in well-fed animals (Figure 4B), and the levels of mature *miR-305* were reduced in starved animals that overexpressed *miR-305* in FB cells when compared to normally fed animals of the same genotype (Figure 5E). These results indicate that processing of *miR-305* is compromised in starvation.

We then determined whether systemic or FB-specific depletion of the miRNA processing machinery increased the survival rates of adult flies subjected to starvation and whether this extension relied on the activity of Dp53. Halving the doses of the *dcr-1* gene ($dcr\text{-}1^{Q1147X}$/+ flies show reduced levels of mature miRNAs including *miR-305*; Figure S4), or having the doses of the *miR-305* locus (in *Df-miR-305*/+ flies) increased the survival rates of both males and female adult flies subjected to nutrient starvation when compared to *control* flies (Figures 6A–6D and 6I; Table S1). The levels of TAGs and glycogen were increased in both genotypes at the beginning of the starvation procedure, and the consumption of energy resources was delayed with time (Figure S4). This is most likely a consequence of increased levels of Dp53 activity and the proposed role of Dp53 in reducing glycolysis in FB cells, as halving the doses of the *dp53* gene reverted the survival rates of *dcr-1* heterozygous flies (in $dcr\text{-}1^{Q1147X}/dp53^{ns}$ flies; Figure 6I). Targeted expression of a dsRNA form of *dcr-1* in FB cells (in $ppl > dcr\text{-}1^{RNAi}$ flies) also increased starvation resistance (Figures 6E and 6F; Table S1), and the extended survival rates were reverted upon coexpression of a dominant-negative version of Dp53 (in $ppl > dcr\text{-}1^{RNAi}$, $dp53^{H159.N}$ flies; Figures 6G and 6H). Parental UAS lines ($UAS\text{-}dcr\text{-}1^{RNAi}$, and $UAS\text{-}dcr\text{-}1^{RNAi}$ $UAS\text{-}dp53^{H159.N}$) showed similar survival rates upon fasting than control UAS-GFP flies (Figure S4; Table S1). Altogether, these results indicate that depletion of nutrients reduces the activity of the miRNA machinery in FB cells and as a consequence alleviates *miR-305*-mediated targeting of *dp53,* which eventually contributes to organismal resistance to nutrient deprivation.

DISCUSSION

The tumor suppressor gene p53 has been reported to mediate metabolic changes in cells through the regulation of several metabolic pathways and can promote cell survival upon nutrient deprivation (Maddocks et al., 2013; Vousden and Ryan, 2009). Here, we provide evidence that *Drosophila* p53 participates in organismal adaptation to nutrient deprivation and exerts its function by modulating the breakdown of energy resources in FB cells. The response of an organism to metabolic stress, such as starvation, is largely dependent on its capacity to derive energy from stored reserves like TAGs and glycogen (Arrese and Soulages, 2010). Energy storage in FB cells is known to be modulated by the combined action of dILPs and AKH. In

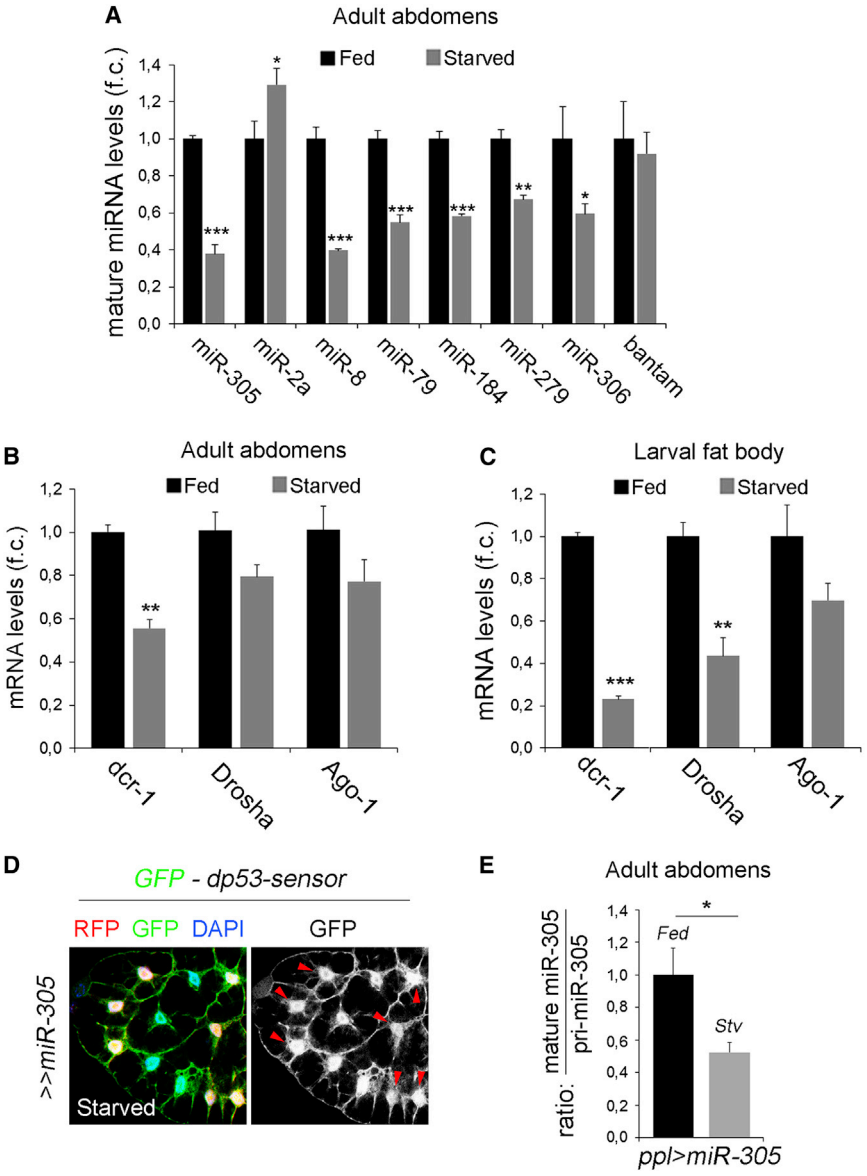

Figure 5. Reduced Activity of the miRNA Pathway Caused by Nutrient Deprivation

(A–C) Histograms plotting mature miRNAs levels (A) or Drosha, Dicer-1, and Argonaute-1 expression levels (B and C) measured by quantitative RT-PCR of adult abdomens (A and B) or larval FBs (C) of fed (black bars) or starved (gray bars) control animals. Results are expressed as fold induction with respect to fed conditions.

(D) FB cells of starved animals overexpressing RFP and *miR-305*, carrying the *dp53-sensor*, and stained to visualize EGFP (green) protein expression. Note that *miR-305* overexpression did not reduce EGFP levels under these circumstances (compare with well-fed animals shown in Figure 4B).

(E) Histograms plotting the ratio between mature and primary *miR-305* levels measured by quantitative RT-PCR of adult abdomens of fed (black bar) or starved (gray bar) animals overexpressing *miR-305* in the FB (*ppl>miR-305*). Results are expressed as fold induction with respect to fed conditions.

Error bars represent SEM. ***$p < 0.001$, **$p < 0.01$ and *$p < 0.05$. See also Table S2.

well-fed animals, insulin signaling promotes energy storage, whereas during fasting periods, AKH and reduced levels of circulating dILPs contribute to the mobilization of energy resources (Bharucha et al., 2008; Kim and Rulifson, 2004; Rulifson et al., 2002). The changes in insulin signaling and AKH expression produced by nutrient deprivation were very similar in *Dp53*-depleted and control animals. Moreover, and consistent with the accelerated TAG consumption observed in starved *dp53* mutant flies, specific depletion of Dp53 activity in single FB cells caused smaller lipid droplets. Altogether, these observations support the notion that Dp53 has a cell-autonomous activity in FB cells, which impacts the rates of energy resources breakdown upon nutrient deprivation. The activity of Dp53 in FB cells also promotes organismal survival upon nutrient deprivation. Reduced survival rates of fasting *dp53* mutant animals are most probably a consequence of reduced amount of sugar in the animal, as increasing the concentration of sugar in the food rescued the survival rates of fasting *dp53* mutant animals.

The accelerated consumption of energy resources observed in starved *Dp53*-depleted animals does not appear to be a consequence of altered changes in metabolic enzymes involved in mobilizing these resources. Fasting also induces a decrease in the levels of enzymes involved in glycolysis, cellular respiration, and fatty acid β-oxidation. Reduced rates of glucose and fatty acid catabolism in starved FB cells might reflect a preferential use of these metabolites for the production of circulating sugars and lipids to be used by peripheral tissues upon starvation. Interestingly, the levels of the glycolytic enzymes PGM and Hex-C are reduced in control animals upon fasting but remain unchanged in *dp53* mutant flies. These results most probably reflect a defective functional specialization of *dp53* mutant FB cells toward the production of sugars in fasting conditions and support a role of Dp53 in metabolic adaptation to nutrient deprivation. Of note, PGM is negatively regulated by p53 in cultured mammalian cells (Kondoh et al., 2005), suggesting a conserved role of p53 in regulating glycolysis in vertebrate and invertebrate tissues.

In the last few years, the expression of p53 has been shown to be under the control of miRNAs (Hermeking, 2012). We have analyzed the involvement of the miRNA machinery in targeting *dp53* in normal physiological conditions and upon nutritional starvation. We present evidence that, in normal physiological conditions, the miRNA machinery targets the *dp53 3′UTR* and have identified *miR-305* as a major regulatory element. Nutrient

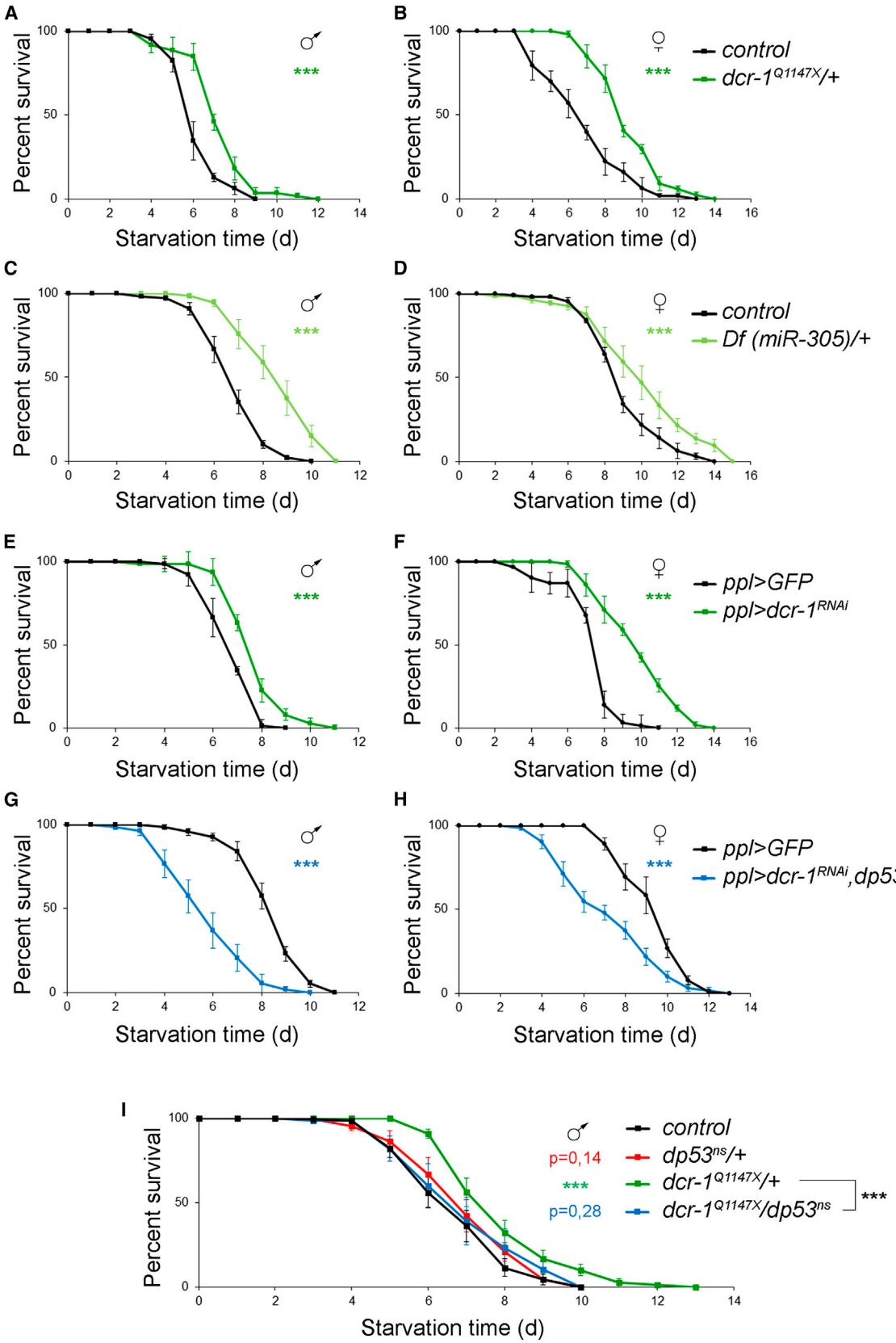

(legend on next page)

conditions modulate the capacity of the miRNA machinery to target Dp53, as nutrient deprivation, depletion of the Slimfast amino acid transporter, or reduced activity of TOR signaling diminishes the ability of *miR-305* to target the *dp53 3′UTR.* Although these results open up the possibility of a specific modulation of *miR-305* levels by nutrition, our findings unravel a general downregulation of miRNA levels in fasted FB cells. Thus, the expression levels of Drosha and Dicer, involved in miRNA processing, and Ago1, a component of RISC, were downregulated upon nutrient deprivation. A similar impact on the activity of the whole miRNA machinery has been observed under several stress conditions, including hypoxia, autophagy, UV radiation, and oxidative stress (Blandino et al., 2012; Gibbings et al., 2012; Ho et al., 2012). Thus, stress-induced depletion of the miRNA machinery appears to be a conserved mechanism that contributes to the derepression of certain genes involved in the biological responses to the original stress, in this particular case to nutrient deprivation.

The miRNA machinery was previously shown to promote tissue growth by targeting the *Drosophila* ortholog of the TRIM32 tumor suppressor gene Mei-P26, which triggers proteasome-dependent degradation of the proto-oncogene dMyc (Herranz et al., 2010). Increased levels of Mei-P26 target dMyc protein for degradation, thus reducing the capacity of the tissue to increase cellular mass. In addition, the conserved miRNA *miR-8* and its target, *USH*, regulate body size in *Drosophila* (Hyun et al., 2009). USH is a negative regulator of the PI3K signaling pathway, and overexpression of *miR-8* in FB cells activates PI3K and promotes growth cell autonomously. The identification of Dp53 as a critical element modulating the consumption of energy resources in FB cells and its regulation by the miRNA machinery point to a central role of miRNAs in coordinating the cellular and physiological responses to nutritional starvation. In response to nutrient deprivation, downregulation of Dicer-1, Drosha, and Ago1 levels result in a general reduction of active mature miRNAs in FB cells, thus contributing to the expected decrease in the activity of growth-promoting genes (dMyc) or pathways (PI3K) and a concomitant increase in the activity of genes, such as *dp53*, that modulate the rates of glycogen and TAG catabolism.

Amino acid sensing by TOR in FB cells regulates, through Upd/JAK-STAT signaling, the rates of dILPs secretion in the insulin-producing cells (Géminard et al., 2009; Rajan and Perrimon, 2012), which in turn modulate, through the insulin-like receptor signaling pathway, fat cell mass in adult flies (adipocyte cell number and TAGs storage; DiAngelo and Birnbaum, 2009). Our study indicates that amino acid sensing by TOR also regulates Dp53 activity levels in FB cells and that Dp53 promotes, upon starvation, a functional specialization of FB cells toward the production of sugars and fatty acids to be used by the peripheral tissues. Thus, TOR and FB cells appear to play a fundamental role in coordinating the organismal response to starvation by sensing amino acid availability in the food.

EXPERIMENTAL PROCEDURES

Drosophila Genetics, Antibodies, and Constructs

Flies were raised at 25°C in standard medium (4% glucose, 55 g/l yeast, 0.65% agar, 28 g/l wheat flour, 4 ml/l propionic acid, and 1.1 g/l Nipagin). Fly stocks, mosaic analysis, constructs, antibodies, and immunohistochemistry are described in the Supplemental Experimental Procedures.

Starvation Treatments

Starvation procedures were adapted from (Rajan and Perrimon, 2012).

For starvation sensitivity assays, 15–20 (1- to 2-day-old) flies of each genotype were transferred into vials containing 2% agar and 1% sucrose. Flies were transferred to new tubes every day, and dead flies were counted. At least 100 flies per genotype were scored. Control animals were always analyzed in parallel in each experimental condition. Statistics were performed using GraphPad Prism 4.0 software, which uses the Kaplan-Meier estimator to calculate survival fractions as well as median and maximum survival values. Curves were compared using the log-rank (Mantel-Cox) test. The two-tailed p value indicates the value of the difference between the two entire survival distributions at comparison.

For starvation treatments in adults, 5- to 7-day-old flies were used and subjected to 24 hr (for glycogen and trehalose measurements and for expression analyses) or 72 hr (for TAG measurements) of starvation.

For starvation treatments in larvae, animals were synchronized in the second to third larval transition and placed 6 hr later in tubes with 2% agar 1% sucrose (starvation) or standard food (fed). After 24–48 hr, FBs were dissected and used for immunohistochemistry or RNA extraction.

Metabolic Assays

TAG, glycogen, and trehalose levels were performed as previously described (Palanker et al., 2009). Briefly, five adult males were homogenized in 200 μl of the corresponding buffers and immediately incubated at 70°C for 5 min to inactivate endogenous enzymes. For quantification of sugars in circulation, hemolymph was pooled from 40–45 adult flies to obtain 1 μl for assay, diluted 1:100, and incubated at 70°C for 5 min. For TAG assays, samples were assayed using a serum triglyceride determination kit (Sigma-Aldrich, TR0100) according to the manufacturer's protocol. For glycogen and trehalose measurements, samples were incubated with or without 1 U of Amyloglucosidase (Sigma-Aldrich, A7420, for glycogen) or with 0.05 U/ml of trehalase (Sigma-Aldrich, T8778, for trehalose) for 2 hr at 37°C and assayed using a Glucose (GO) Assay Kit (GAGO-20). Metabolite measurements were normalized to protein concentration (Bio-Rad). Five replicates for each genotype and condition were performed, and data were normalized with respect to the corresponding levels in control flies. Further details are in the Supplemental Experimental Procedures.

Quantitative RT-PCR

For the quantification of mRNA levels, total RNA was extracted using TRIzol reagent (Invitrogen) from FBs of ten larvae, abdomens of ten adult males, five decapitated adult males, or five heads, depending on the experiment. A total of 2 μg of total RNA was used as a template for cDNA synthesis using Maxima Reverse Transcriptase (Thermo Scientific). Maxima SYBR Green/ROX qPCR Master Mix (Thermo Scientific) was used, and reactions were run in a Light Cycler 480 Real Time qPCR machine (Roche). Transcript levels were normalized to tubulin. The primer pairs used are tabulated in Table S2.

Figure 6. Increased Starvation Resistance upon FB-Specific Depletion of the miRNA Machinery

Survival rates to nutrient deprivation (2% agar, 1% sucrose) of young adult flies of the genotypes *dicer*^{Q1147X}/+ (A, B, and I), *Df(miR-305)*/+ (C and D), *ppl-gal4; UAs-dcr-1*^{RNAI} (E and F), *ppl-gal4, UAS-dcr-1*^{RNAi}, *UAS-dp53*$^{H159.N}$ (G and H), *dp53*^{ns}/+ (I), and *dicer*^{Q1147X}/*dp53*^{ns} compared to control flies (black lines) of the genotypes *FRT82B ry*^{506}/+ (A and B), *w*^{1118} (C, D, and I), and *ppl-gal4; UAS-GFP* (E–H) subjected to the same procedure. Both males (A, C, E, G, and I) and females (B, D, F, and H) are shown. See Table S1 for n, p, median, and maximum survival values. Error bars represent SEM. ***$p < 0.001$. The p value tests the null hypothesis that the survival curves are identical.

See also Figure S4 and Table S1.

For quantification of mature miRNA levels, total RNA was extracted from the abdomens of ten adult flies with TRIzol reagent (Invitrogen). A total of 10 ng of RNA was used as a template for miRNA-specific cDNA synthesis (Applied Biosystems). miRNAs was quantified using TaqMan miRNA assays (Applied Biosystems). Snor442 and U27 were used for normalization.

In all cases, three independent samples were collected from each condition and genotype, and duplicate measurements were conducted.

SUPPLEMENTAL INFORMATION

Supplemental Information includes Supplemental Experimental Procedures, four figures, and two tables and can be found with this article online at http://dx.doi.org/10.1016/j.celrep.2014.06.020.

AUTHOR CONTRIBUTIONS

L.B., A.D., and M.M. conceived and designed the experiments. L.B. and A.D. performed the experiments. L.B., A.D., and M.M. analyzed the data. M.M. wrote the paper, and all authors approved the final version of the manuscript.

ACKNOWLEDGMENTS

We thank J. Abrams, J. Colombani, S. Cohen, R. Delanue, E. Izaurralde, H. Jasper, P. Leopold, N. Perrimon, A. Teleman, J.M. Reichhart, the Bloomington Stock Center, the Developmental Studies Hybridoma Bank, and the Vienna Drosophila RNAi Center for flies and reagents; T. Yates for text editing; and H. Stocker, A. Teleman, A. Ferreira, and L. Boulan for comments on the manuscript. L.B. and A. D. are funded by a FPI predoctoral fellowship and a Juan de la Cierva postdoctoral contract, respectively, from the Spanish Ministerio de Economía y Competitividad. M.M. is an ICREA Research Professor, and this work was funded by BFU2010-21123, CSD2007-00008, and 2005 SGR 00118 grants.

Received: January 29, 2014
Revised: May 27, 2014
Accepted: June 16, 2014
Published: July 10, 2014

REFERENCES

Arrese, E.L., and Soulages, J.L. (2010). Insect fat body: energy, metabolism, and regulation. Annu. Rev. Entomol. *55*, 207–225.

Bauer, J.H., and Helfand, S.L. (2009). Sir2 and longevity: the p53 connection. Cell Cycle *8*, 1821.

Berkers, C.R., Maddocks, O.D., Cheung, E.C., Mor, I., and Vousden, K.H. (2013). Metabolic regulation by p53 family members. Cell Metab. *18*, 617–633.

Bharucha, K.N., Tarr, P., and Zipursky, S.L. (2008). A glucagon-like endocrine pathway in Drosophila modulates both lipid and carbohydrate homeostasis. J. Exp. Biol. *211*, 3103–3110.

Blandino, G., Valerio, M., Cioce, M., Mori, F., Casadei, L., Pulito, C., Sacconi, A., Biagioni, F., Cortese, G., Galanti, S., et al. (2012). Metformin elicits anticancer effects through the sequential modulation of DICER and c-MYC. Nat Commun *3*, 865.

Brand, A.H., and Perrimon, N. (1993). Targeted gene expression as a means of altering cell fates and generating dominant phenotypes. Development *118*, 401–415.

Brennecke, J., Hipfner, D.R., Stark, A., Russell, R.B., and Cohen, S.M. (2003). bantam encodes a developmentally regulated microRNA that controls cell proliferation and regulates the proapoptotic gene hid in Drosophila. Cell *113*, 25–36.

Brodsky, M.H., Nordstrom, W., Tsang, G., Kwan, E., Rubin, G.M., and Abrams, J.M. (2000). Drosophila p53 binds a damage response element at the reaper locus. Cell *101*, 103–113.

Canavoso, L.E., Jouni, Z.E., Karnas, K.J., Pennington, J.E., and Wells, M.A. (2001). Fat metabolism in insects. Annu. Rev. Nutr. *21*, 23–46.

Colombani, J., Raisin, S., Pantalacci, S., Radimerski, T., Montagne, J., and Léopold, P. (2003). A nutrient sensor mechanism controls Drosophila growth. Cell *114*, 739–749.

Demontis, F., and Perrimon, N. (2010). FOXO/4E-BP signaling in Drosophila muscles regulates organism-wide proteostasis during aging. Cell *143*, 813–825.

DiAngelo, J.R., and Birnbaum, M.J. (2009). Regulation of fat cell mass by insulin in Drosophila melanogaster. Mol. Cell. Biol. *29*, 6341–6352.

Géminard, C., Rulifson, E.J., and Léopold, P. (2009). Remote control of insulin secretion by fat cells in Drosophila. Cell Metab. *10*, 199–207.

Gibbings, D., Mostowy, S., Jay, F., Schwab, Y., Cossart, P., and Voinnet, O. (2012). Selective autophagy degrades DICER and AGO2 and regulates miRNA activity. Nat. Cell Biol. *14*, 1314–1321.

Grewal, S.S. (2009). Insulin/TOR signaling in growth and homeostasis: a view from the fly world. Int. J. Biochem. Cell Biol. *41*, 1006–1010.

Grönke, S., Mildner, A., Fellert, S., Tennagels, N., Petry, S., Müller, G., Jäckle, H., and Kühnlein, R.P. (2005). Brummer lipase is an evolutionary conserved fat storage regulator in Drosophila. Cell Metab. *1*, 323–330.

Gu, B., and Zhu, W.G. (2012). Surf the post-translational modification network of p53 regulation. Int. J. Biol. Sci. *8*, 672–684.

Hennig, K.M., and Neufeld, T.P. (2002). Inhibition of cellular growth and proliferation by dTOR overexpression in Drosophila. Genesis *34*, 107–110.

Herranz, H., Hong, X., Pérez, L., Ferreira, A., Olivieri, D., Cohen, S.M., and Milán, M. (2010). The miRNA machinery targets Mei-P26 and regulates Myc protein levels in the Drosophila wing. EMBO J. *29*, 1688–1698.

Hermeking, H. (2012). MicroRNAs in the p53 network: micromanagement of tumour suppression. Nat. Rev. Cancer *12*, 613–626.

Hietakangas, V., and Cohen, S.M. (2009). Regulation of tissue growth through nutrient sensing. Annu. Rev. Genet. *43*, 389–410.

Ho, J.J., Metcalf, J.L., Yan, M.S., Turgeon, P.J., Wang, J.J., Chalsev, M., Petruzziello-Pellegrini, T.N., Tsui, A.K., He, J.Z., Dhamko, H., et al. (2012). Functional importance of Dicer protein in the adaptive cellular response to hypoxia. J. Biol. Chem. *287*, 29003–29020.

Huntzinger, E., and Izaurralde, E. (2011). Gene silencing by microRNAs: contributions of translational repression and mRNA decay. Nat. Rev. Genet. *12*, 99–110.

Hyun, S., Lee, J.H., Jin, H., Nam, J., Namkoong, B., Lee, G., Chung, J., and Kim, V.N. (2009). Conserved MicroRNA miR-8/miR-200 and its target USH/FOG2 control growth by regulating PI3K. Cell *139*, 1096–1108.

Jiang, P., Du, W., and Yang, X. (2013). p53 and regulation of tumor metabolism. J. Carcinog. *12*, 21.

Jin, S., Martinek, S., Joo, W.S., Wortman, J.R., Mirkovic, N., Sali, A., Yandell, M.D., Pavletich, N.P., Young, M.W., and Levine, A.J. (2000). Identification and characterization of a p53 homologue in Drosophila melanogaster. Proc. Natl. Acad. Sci. USA *97*, 7301–7306.

Jones, R.G., Plas, D.R., Kubek, S., Buzzai, M., Mu, J., Xu, Y., Birnbaum, M.J., and Thompson, C.B. (2005). AMP-activated protein kinase induces a p53-dependent metabolic checkpoint. Mol. Cell *18*, 283–293.

Kim, S.K., and Rulifson, E.J. (2004). Conserved mechanisms of glucose sensing and regulation by Drosophila corpora cardiaca cells. Nature *431*, 316–320.

Kondoh, H., Lleonart, M.E., Gil, J., Wang, J., Degan, P., Peters, G., Martinez, D., Carnero, A., and Beach, D. (2005). Glycolytic enzymes can modulate cellular life span. Cancer Res. *65*, 177–185.

Kühnlein, R.P. (2012). Thematic review series: Lipid droplet synthesis and metabolism: from yeast to man. Lipid droplet-based storage fat metabolism in Drosophila. J. Lipid Res. *53*, 1430–1436.

Lane, D.P., and Verma, C. (2012). Mdm2 in evolution. Genes Cancer *3*, 320–324.

Lee, Y., Ahn, C., Han, J., Choi, H., Kim, J., Yim, J., Lee, J., Provost, P., Rådmark, O., Kim, S., and Kim, V.N. (2003). The nuclear RNase III Drosha initiates microRNA processing. Nature *425*, 415–419.

Lu, W.J., Chapo, J., Roig, I., and Abrams, J.M. (2010). Meiotic recombination provokes functional activation of the p53 regulatory network. Science *328*, 1278–1281.

Maddocks, O.D., Berkers, C.R., Mason, S.M., Zheng, L., Blyth, K., Gottlieb, E., and Vousden, K.H. (2013). Serine starvation induces stress and p53-dependent metabolic remodelling in cancer cells. Nature *493*, 542–546.

Mandal, S., Guptan, P., Owusu-Ansah, E., and Banerjee, U. (2005). Mitochondrial regulation of cell cycle progression during development as revealed by the tenured mutation in Drosophila. Dev. Cell *9*, 843–854.

Mandal, S., Freije, W.A., Guptan, P., and Banerjee, U. (2010). Metabolic control of G1-S transition: cyclin E degradation by p53-induced activation of the ubiquitin-proteasome system. J. Cell Biol. *188*, 473–479.

Ollmann, M., Young, L.M., Di Como, C.J., Karim, F., Belvin, M., Robertson, S., Whittaker, K., Demsky, M., Fisher, W.W., Buchman, A., et al. (2000). Drosophila p53 is a structural and functional homolog of the tumor suppressor p53. Cell *101*, 91–101.

Palanker, L., Tennessen, J.M., Lam, G., and Thummel, C.S. (2009). Drosophila HNF4 regulates lipid mobilization and beta-oxidation. Cell Metab. *9*, 228–239.

Puig, O., Marr, M.T., Ruhf, M.L., and Tjian, R. (2003). Control of cell number by Drosophila FOXO: downstream and feedback regulation of the insulin receptor pathway. Genes Dev. *17*, 2006–2020.

Rajan, A., and Perrimon, N. (2012). Drosophila cytokine unpaired 2 regulates physiological homeostasis by remotely controlling insulin secretion. Cell *151*, 123–137.

Ranganayakulu, G., Zhao, B., Dokidis, A., Molkentin, J.D., Olson, E.N., and Schulz, R.A. (1995). A series of mutations in the D-MEF2 transcription factor reveal multiple functions in larval and adult myogenesis in Drosophila. Dev. Biol. *171*, 169–181.

Ruby, J.G., Stark, A., Johnston, W.K., Kellis, M., Bartel, D.P., and Lai, E.C. (2007). Evolution, biogenesis, expression, and target predictions of a substantially expanded set of Drosophila microRNAs. Genome Res. *17*, 1850–1864.

Rulifson, E.J., Kim, S.K., and Nusse, R. (2002). Ablation of insulin-producing neurons in flies: growth and diabetic phenotypes. Science *296*, 1118–1120.

Scherz-Shouval, R., Weidberg, H., Gonen, C., Wilder, S., Elazar, Z., and Oren, M. (2010). p53-dependent regulation of autophagy protein LC3 supports cancer cell survival under prolonged starvation. Proc. Natl. Acad. Sci. USA *107*, 18511–18516.

Teleman, A.A., Chen, Y.W., and Cohen, S.M. (2005). 4E-BP functions as a metabolic brake used under stress conditions but not during normal growth. Genes Dev. *19*, 1844–1848.

Toledo, F., and Wahl, G.M. (2006). Regulating the p53 pathway: in vitro hypotheses, in vivo veritas. Nat. Rev. Cancer *6*, 909–923.

Ugrankar, R., Liu, Y., Provaznik, J., Schmitt, S., and Lehmann, M. (2011). Lipin is a central regulator of adipose tissue development and function in Drosophila melanogaster. Mol. Cell. Biol. *31*, 1646–1656.

Vousden, K.H., and Ryan, K.M. (2009). p53 and metabolism. Nat. Rev. Cancer *9*, 691–700.

Waskar, M., Landis, G.N., Shen, J., Curtis, C., Tozer, K., Abdueva, D., Skvortsov, D., Tavaré, S., and Tower, J. (2009). Drosophila melanogaster p53 has developmental stage-specific and sex-specific effects on adult life span indicative of sexual antagonistic pleiotropy. Aging (Albany, N.Y. Online) *1*, 903–936.

Cell Reports, Volume *8*

Supplemental Information

MicroRNA-Mediated Regulation of Dp53 in the *Drosophila* Fat Body Contributes to Metabolic Adaptation to Nutrient Deprivation

Lara Barrio, Andrés Dekanty, and Marco Milán

Supplemental Figures

Figure S1

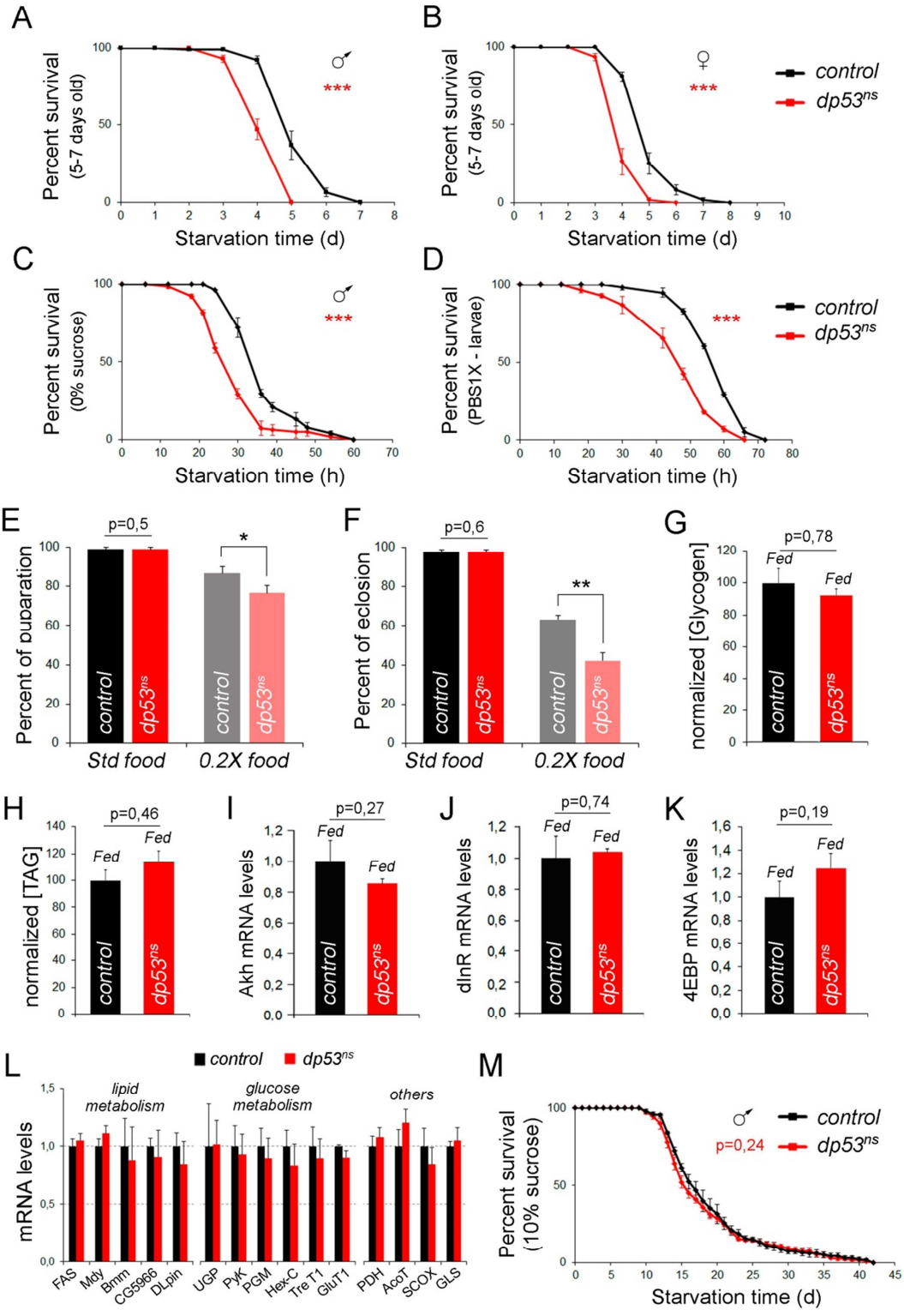

Figure S1. Related to Figure 1

(A, B) Survival rates to nutrient deprivation (2% agar, 1% sucrose) of 5-7-day-old *dp53* mutant (*dp53*^{ns}) and control (*w*^{1118}) adult flies.Both males (A) and females (B) are shown. See Table S1 for n, p, median and maximum survival values.

(C) Survival rates to complete nutrient deprivation (2% agar, 0% sucrose) of 1-2-day-old *dp53* mutant (*dp53*^{ns}) and control (*w*^{1118}) adult males. See Table S1 for n, p, median and maximum survival values.

(D) Survival rates to nutrient deprivation (PBS1X soaked paper) of *dp53* mutant (*dp53*^{ns}) and control (*w*^{1118}) larvae. See Table S1 for n, p, median and maximum survival values.

(E, F) Histograms plotting percent of pupariation (E) and eclosion (F) of control (*w*^{1118}) and *dp53*^{ns} mutant larvae raised immediately after haching in standard food (Std food) or in diluted food (0.2X food). Data were represented as a percent of the fed values for each genotype.

(G, H) Histograms plotting glycogen (G) and TAG (H) levels from adult male *dp53* mutant (*dp53*^{ns}) and control (*w*^{1118}) flies under well-fed conditions. Data were normalized to protein concentration and represented as a percentage of the control (*w*^{1118}) values.

(I-K) Histograms plotting Akh (I), dInR (J) and 4EBP (K) mRNA levels from heads (I) or bodies (J, K) in *dp53* mutant (*dp53*^{ns}) and control (*w*^{1118}) adult males under well-fed conditions.

(L) Histogram plotting mRNA levels of a collection of fifteen key metabolic enzymes in *dp53* mutant (*dp53*^{ns}) and control (*w*^{1118}) adult males under well-fed conditions.

mRNA levels in I-K are expressed as fold induction with respect to *control* animals.

(M) Survival rates to nutrient deprivation (2% agar, 10% sucrose) of 1-2-day-old *dp53* mutant (*dp53*^{ns}) and control (*w*^{1118}) adult males. See Table S1 for n, p, median and maximum survival values. The p-value in panels A-D and M tests the null hypothesis that the survival curves are identical.

Error bars represent SEM. *** $p<0.001$, ** $p<0.01$ and * $p<0.05$.

Figure S2

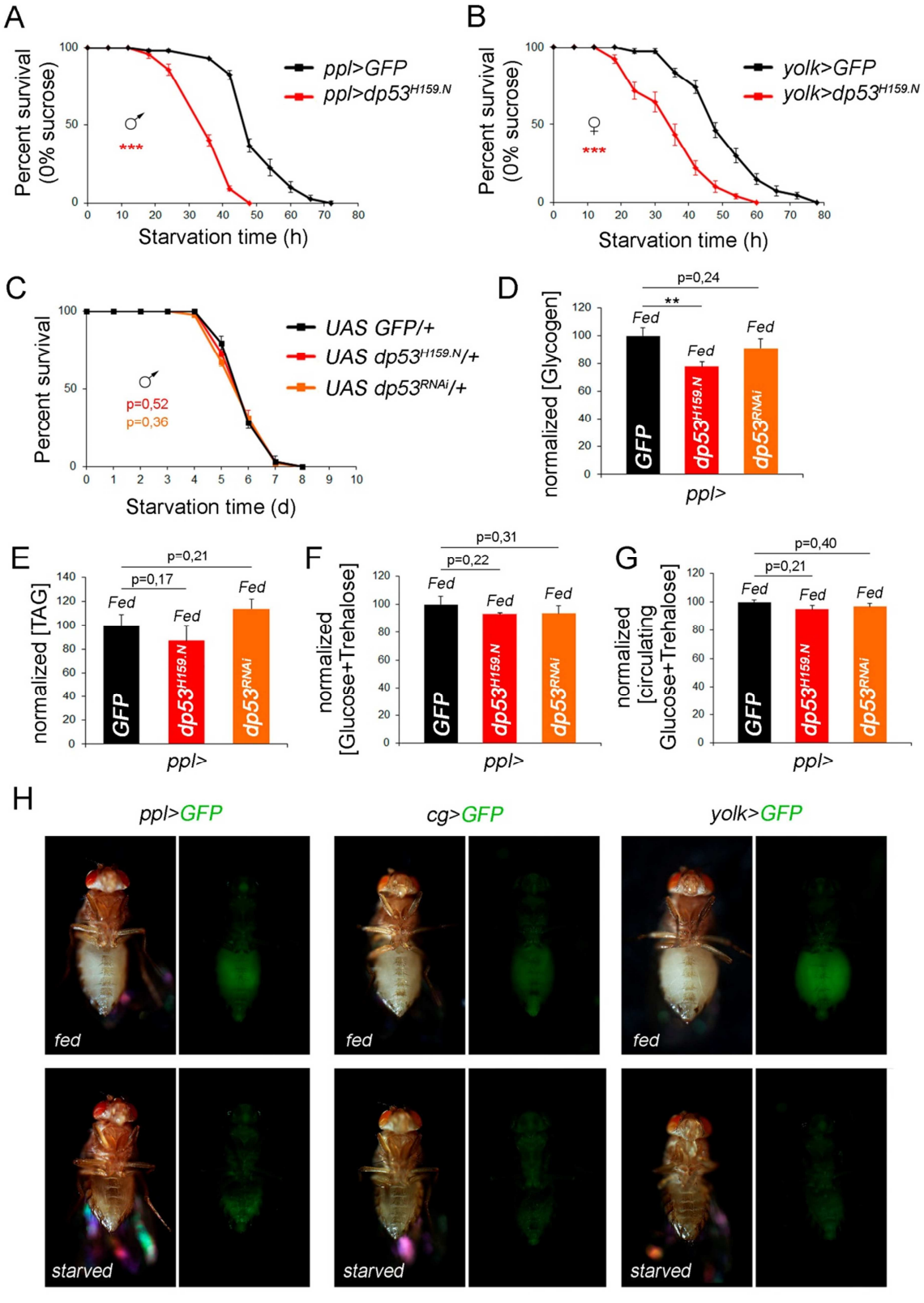
A
Percent survival (0% sucrose)
ppl>GFP
ppl>dp53H159.N
♂
***
Starvation time (h)
B
Percent survival (0% sucrose)
yolk>GFP
yolk>dp53H159.N
♀
***
Starvation time (h)
C
Percent survival
UAS GFP/+
UAS dp53H159.N/+
UAS dp53RNAi/+
♂
p=0,52
p=0,36
Starvation time (d)
D
normalized [Glycogen]
p=0,24
**
Fed
GFP
dp53H159.N
dp53RNAi
ppl>
E
normalized [TAG]
p=0,21
p=0,17
Fed
GFP
dp53H159.N
dp53RNAi
ppl>
F
normalized [Glucose+Trehalose]
p=0,31
p=0,22
Fed
GFP
dp53H159.N
dp53RNAi
ppl>
G
normalized [circulating Glucose+Trehalose]
p=0,40
p=0,21
Fed
GFP
dp53H159.N
dp53RNAi
ppl>
H
ppl>GFP
cg>GFP
yolk>GFP
fed
starved

Figure S2. Related to Figure 2

(A-C) Survival rates to nutrient deprivation (2% agar, 0% sucrose in A and B, and 2% agar, 1% sucrose in C) of 1-2-day-old adult flies of the corresponding indicated genotypes. See Table S1 for n, p, median and maximum survival values. The p-value tests the null hypothesis that the survival curves are identical.

(D-G) Histograms plotting whole body glycogen (D), TAG (E) and total glucose+trehalose (F) or hemolymph glucose+trehalose (G) levels from adult males expressing *GFP*, $dp53^{H159.N}$ or $dp53^{RNAi}$ in FB cells under well-fed conditions. Data were normalized to protein concentration (D-F) or to µl of hemolymph and represented as a percentage of the control (w^{1118}) values.

Error bars represent SEM. *** $p<0.001$ and ** $p<0.01$.

(H) Representative images of adult females expressing GFP under the indicated FB-gal4 drivers in well-fed and starved (for five days) conditions. Identical fluorescence settings and all subsequent treatments of images were used to allow direct comparison between different conditions.

Figure S3

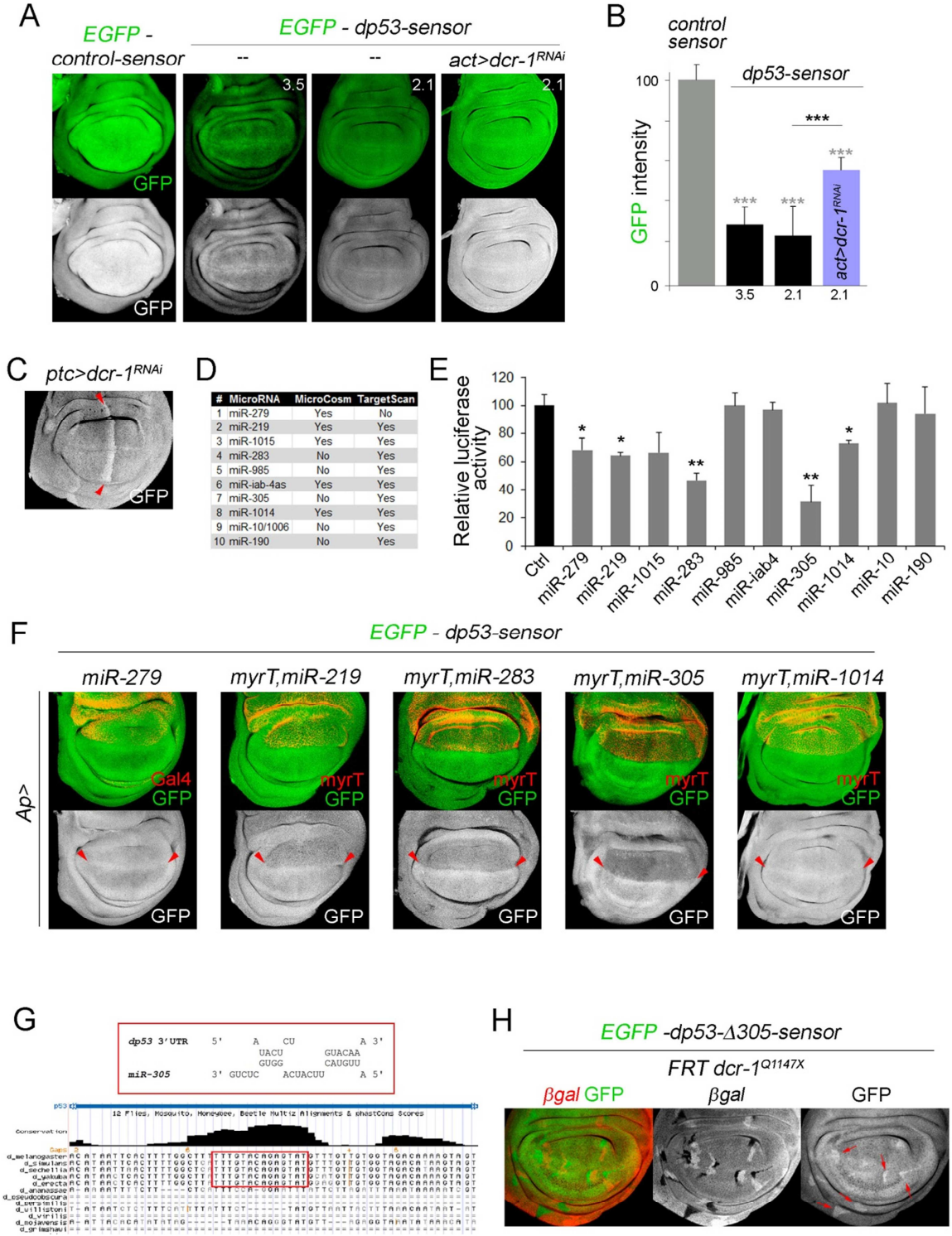
A
EGFP - control-sensor
EGFP - dp53-sensor
--
--
act>dcr-1RNAi
3.5
2.1
2.1
GFP
GFP
B
control sensor
dp53-sensor
GFP intensity
100
0
***
***
***
***
3.5
2.1
2.1
act>dcr-1RNAi
C
ptc>dcr-1RNAi
GFP
D
MicroRNA MicroCosm TargetScan
1 miR-279 Yes No
2 miR-219 Yes Yes
3 miR-1015 Yes Yes
4 miR-283 No Yes
5 miR-985 No Yes
6 miR-iab-4as Yes Yes
7 miR-305 No Yes
8 miR-1014 Yes Yes
9 miR-10/1006 No Yes
10 miR-190 No Yes
E
Relative luciferase activity
120
100
80
60
40
20
0
*
*
**
**
*
Ctrl
miR-279
miR-219
miR-1015
miR-283
miR-985
miR-iab4
miR-305
miR-1014
miR-10
miR-190
F
EGFP - dp53-sensor
miR-279
myrT,miR-219
myrT,miR-283
myrT,miR-305
myrT,miR-1014
Ap>
Gal4 GFP
myrT GFP
GFP
G
dp53 3'UTR 5' A CU A 3'
UACU GUACAA
GUGG CAUGUU
miR-305 3' GUCUC ACUACUU A 5'
12 Flies, Mosquito, Honeybee, Beetle Multiz Alignments & phastCons Scores
Conservation
d_melanogaster
d_simulans
d_sechellia
d_yakuba
d_erecta
d_ananassae
d_pseudoobscura
d_persimilis
d_willistoni
d_virilis
d_mojavensis
d_grimshawi
H
EGFP -dp53-Δ305-sensor
FRT dcr-1Q1147X
βgal GFP
βgal
GFP

Figure S3. Related to Figure 3

(A) Wing discs carrying the *control-sensor* (left panels) or two independent transgenic lines carrying the *dp53-sensor* (3.5 and 2.1) imaged with identical confocal microscope settings and processed identically to allow direct comparison. Also, *actin-gal4;UAS-dcr-1*^{RNAi} wing discs carrying the *dp53-sensor* (line 2.1) is shown.

(B) Histogram plotting EGFP expression levels of wing discs shown in A. Note decreased levels of the *dp53-sensor* relative to the *control-sensor* and increased levels of the *dp53-sensor* upon *dcr-1*^{RNAi} expression.

(C) Wing disc carrying the *dp53-sensor* and expressing *dcr-1*^{RNAi} under the control of the *ptc-Gal4* driver stained for EGFP (grey) protein expression.

(D) List of predicted miRNA binding sites in the *dp53 3'UTR* obtained by using MicroCosm and TargetScan softwares.

(E) Luciferase assays in S2 cells co-transfected with the dp53-luciferase reporter and individual miRNAs over-expressing plasmids (see Materials and Methods). Luciferase expression was significantly reduced by the over-expression of miR-279, miR-219, miR-283, miR-305 and miR-1014. A representative experiment from three independent replicates is shown.

(F) Wing discs carrying the *dp53-sensor* and over-expressing the indicated miRNAs and myrTomato (myrT) under the control of *Apterous-gal4* (*Ap>*) driver and stained to visualize EGFP (green) or Gal4 (red) protein expression. Note reduced EGFP levels upon miR-219, miR-283 or miR-305 overexpression. Ap is expressed in the dorsal compartment (D). Red arrowheads depict the D-V boundary.

(G) Cartoon depicting the pairing between the putative binding site of miR-305 in the 3'UTR of dp53 (red box). Note partial conservation of that region in the genome of different *Drosophila* species.

(H) *dcr-1*^{Q1147X} homozygous clones (marked by the absence of *β-gal* labeled in red) showing expression of the *dp53Δ305-sensor* (green). Note increased EGFP expression levels in *dcr-1* mutant cells (red arrows).

Error bars represent SEM. *** p<0.001, ** p<0.01 and * p<0.05.

Figure S4

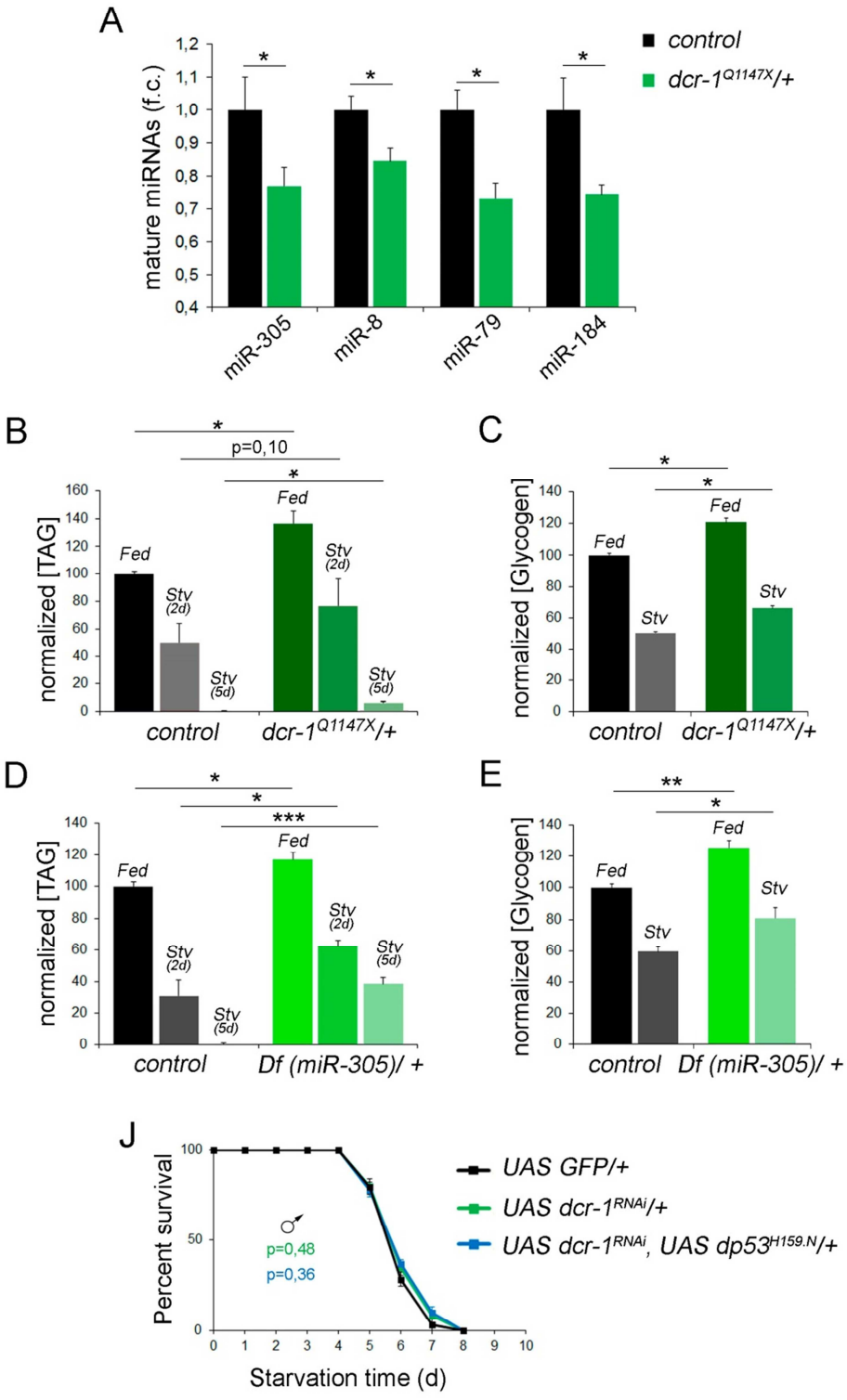
A
mature miRNAs (f.c.)
control
dcr-1Q1147X/+
miR-305
miR-8
miR-79
miR-184
B
normalized [TAG]
p=0,10
Fed
Stv (2d)
Stv (5d)
control
dcr-1Q1147X/+
C
normalized [Glycogen]
Fed
Stv
control
dcr-1Q1147X/+
D
normalized [TAG]
Fed
Stv (2d)
Stv (5d)
control
Df (miR-305)/ +
E
normalized [Glycogen]
Fed
Stv
control
Df (miR-305)/ +
J
Percent survival
p=0,48
p=0,36
UAS GFP/+
UAS dcr-1RNAi/+
UAS dcr-1RNAi, UAS dp53H159.N/+
Starvation time (d)

Figure S4. Related to Figure 6

(A) Histograms plotting mature miRNAs levels measured by quantitative RT-PCR from adult males of *dcr-1* heterozygous *(dcr-1*^{Q1147X}/+) and control (*w*^{1118}) flies. Results are expressed as fold induction with respect to *control* animals.

(B-C) Histograms plotting TAG (B) and glycogen (C) levels from adult male *dcr-1* heterozygous (*dcr-1*^{Q1147X}/+) and control (*w*^{1118}) flies under fed or starved (Stv) conditions. Data were normalized to protein concentration and represented as a percent of the fed values in the *control* individuals.

(D-E) Histograms plotting TAG (D) and glycogen (E) levels from adult male heterozygous for the deficiency covering the miR-305 locus (*Df(miR-305)/*+) and control (*w*^{1118}) flies under fed or starved (Stv) conditions. Data were normalized to protein concentration and represented as a percent of the fed values in the *control* individuals. Animals were starved on 2% agar, 1% for 24 h in C and E, for two (Stv 2d) or five days (Stv 5d) in B and D.

(J) Survival rates to nutrient deprivation (2% agar, 1% sucrose) of young adult flies of the following genotypes: *UAS-GFP*/+, *UAS-dcr-1*^{RNAi}/+, *UAS-dp53*$^{H159.N}$ /+. No significant differences were observed with respect to the control *UAS-GFP* animals. See Table S1 for n, p, median and maximum survival values. The p-value tests the null hypothesis that the survival curves are identical.

Error bars represent SEM. *** p<0.001, ** p<0.01 and * p<0.05.

Supplemental Tables

larvae (PBS1X)	n	Mantel-Cox test	Median surv	Maximum surv
control w^{1118}	116		60 h	72 h
p53^{ns}	118	p < 0,0001	48 h (-20%)	66 h (-9%)
adult males	**n**	**Mantel-Cox test**	**Median surv**	**Maximum surv**
control w^{1118}	130		6	9
p53^{ns}	120	p < 0,0001	4 (-33%)	6 (-33%)
adult females	**n**	**Mantel-Cox test**	**Median surv**	**Maximum surv**
control w^{1118}	136		6	10
p53^{ns}	132	p < 0,0001	4 (-33%)	9 (-10%)
adult males (5-7 d old)	**n**	**Mantel-Cox test**	**Median surv**	**Maximum surv**
control w^{1118}	127		5	7
p53^{ns}	145	p < 0,0001	4 (-20%)	5 (-28%)
adult females (5-7 d old)	**n**	**Mantel-Cox test**	**Median surv**	**Maximum surv**
control w^{1118}	107		5	8
p53^{ns}	101	p < 0,0001	4 (-20%)	6 (-25%)
adult males (0% sucrose	**n**	**Mantel-Cox test**	**Median surv**	**Maximum surv**
control w^{1118}	156		36 h	60 h
p53^{ns}	155	p < 0,0001	30 h (-17%)	60 h (=)
adult males (10% sucros	**n**	**Mantel-Cox test**	**Median surv**	**Maximum surv**
control w^{1118}	125		16	42
p53^{ns}	121	p=0,2447	15 (-6%)	42 (=)
adult males	**n**	**Mantel-Cox test**	**Median surv**	**Maximum surv**
control w^{1118}	107		7	10
p53^{5A14}	101	p < 0,0001	6 (-15%)	8 (-20%)
adult females	**n**	**Mantel-Cox test**	**Median surv**	**Maximum surv**
control w^{1118}	112		9	14
p53^{5A14}	103	p < 0,0001	7 (-22%)	11 (-21%)
adult males	**n**	**Mantel-Cox test**	**Median surv**	**Maximum surv**
control F82B ry^{506} /+	103		6	9
F82B dcr-1Q1147X/+	101	p = 0,0004	7 (+17%)	12 (+33%)
adult females	**n**	**Mantel-Cox test**	**Median surv**	**Maximum surv**
control F82B ry^{506} /+	103		7	13
F82B dcr-1^{Q1147X}/+	104	p < 0,0001	9 (+28%)	14 (+8%)
adult males	**n**	**Mantel-Cox test**	**Median surv**	**Maximum surv**
control w^{1118}	107		7	10
Df (miR-305)/+	100	p< 0,0001	9 (+28%)	11 (+10%)
adult females	**n**	**Mantel-Cox test**	**Median surv**	**Maximum surv**
control w^{1118}	112		9	14
Df (miR-305)/+	105	p< 0,0001	10 (+11%)	15 (+7%)
adult males	**n**	**Mantel-Cox test**	**Median surv**	**Maximum surv**
control w^{1118}	116		7	10
dp53^{ns}/+	142	p=0,1375	7 (=)	10 (=)
dcr-1^{Q1147X}/+	105	p< 0,0001	8 (+14%)	13 (+30%)
dcr-1^{Q1147X}/dp53^{ns}	115	p=0,2812 (*ctrl w^{1118}*)	7 (=)	10 (=)
		p< 0,001 (*dcr-1^{Q1147X}*)		
adult males	**n**	**Mantel-Cox test**	**Median surv**	**Maximum surv**
UAS GFP/+ (control)	108		6	8
UAS dp53$^{H159.N}$/+	104	p = 0,516	6 (=)	8 (=)
UAS dp53^{RNAi}/+	101	p = 0,3649	6 (=)	8 (=)
UAS dcr-1^{RNAi}/+	106	p = 0,475	6 (=)	8 (=)
UAS dcr-1^{RNAi},dp53$^{H159.N}$/	100	p = 0,356	6 (=)	8 (=)

adult males	n	Mantel-Cox test	Median surv	Maximum surv
ppl>GFP (control)	102		4	6
ppl>dp53$^{H159.N}$	100	p < 0,0001	4 (=)	5 (-17%)
ppl>dp53^{RNAi}	100	p < 0,0001	4 (=)	5 (-17%)
adult females	**n**	**Mantel-Cox test**	**Median surv**	**Maximum surv**
ppl>GFP (control)	100		5	7
ppl>dp53$^{H159.N}$	105	p < 0,0001	4 (-20%)	6 (-14%)
ppl>dp53^{RNAi}	101	p < 0,0001	5 (=)	6 (-14%)
adult males (0% sucrose)	**n**	**Mantel-Cox test**	**Median surv**	**Maximum surv**
ppl>GFP (control)	120		48 h	72 h
ppl>dp53$^{H159.N}$	118	p < 0,0001	33 h (-31%)	48 h (-33%)
adult males	**n**	**Mantel-Cox test**	**Median surv**	**Maximum surv**
cg>GFP (control)	100		6	9
cg>dp53$^{H159.N}$	105	p = 0,0004	5 (-17%)	8 (-11%)
cg>dp53^{RNAi}	113	p < 0,0001	5 (-17%)	7 (-22%)
adult females	**n**	**Mantel-Cox test**	**Median surv**	**Maximum surv**
cg>GFP (control)	100		9	12
cg>dp53$^{H159.N}$	105	p < 0,0001	7 (-22%)	9 (-25%)
cg>dp53^{RNAi}	101	p = 0,0303	8 (-11%)	11 (-8%)
adult males	**n**	**Mantel-Cox test**	**Median surv**	**Maximum surv**
mef2>GFP (control)	101		5 (=)	8 (=)
mef2>dp53$^{H159.N}$	100	p = 0,8484	5 (=)	8 (=)
mef2>dp53^{RNAi}	116	p = 0,007	5 (=)	8 (=)
adult females	**n**	**Mantel-Cox test**	**Median surv**	**Maximum surv**
yolk>GFP (control)	103		8	12
yolk>dp53$^{H159.N}$	100	p < 0,0001	5 (-37%)	9 (-25%)
yolk>dp53^{RNAi}	101	p = 0,0321	7 (-12%)	11 (-8%)
adult females	**n**	**Mantel-Cox test**	**Median surv**	**Maximum surv**
yolk>GFP (control)	107		7	10
yolk>dp53$^{2.1}$	101	p < 0,0001	8 (+14%)	12 (+20%)
adult females	**n**	**Mantel-Cox test**	**Median surv**	**Maximum surv**
UASdp53$^{2.1}$/+;dp53^{ns}/+ (cont	103		6	10
yolk>UASdp53$^{2.1}$; p53^{ns}	122	p=0,44	6 (=)	10 (=)
UASdp53$^{2.1}$/+;dp53^{ns}	143	p<0,0001 (*ctrl*)	5 (-16%)	7 (-30%)
		p<0,0001 (*overexp*)		
adult females (0% sucrose)	**n**	**Mantel-Cox test**	**Median surv**	**Maximum surv**
yolk>GFP (control)	110		48 h	78 h
yolk>dp53$^{H159.N}$	115	p < 0,0001	35 h (-27%)	60 h (-23%)
adult males	**n**	**Mantel-Cox test**	**Median surv**	**Maximum surv**
ppl>GFP (control)	108		7	9
ppl>dcr-1^{RNAi}	105	p = 0,0005	8 (+14%)	11 (+22%)
adult females	**n**	**Mantel-Cox test**	**Median surv**	**Maximum surv**
ppl>GFP (control)	100		8	11
ppl>dcr-1^{RNAi}	100	p < 0,0001	10 (+25%)	14 (+27%)
adult males	**n**	**Mantel-Cox test**	**Median surv**	**Maximum surv**
ppl>GFP (control)	106		9	11
ppl>dcr-1^{RNAi},dp53$^{H159.N}$	105	p < 0,0001	6 (-33%)	10 (-9%)
adult females	**n**	**Mantel-Cox test**	**Median surv**	**Maximum surv**
ppl>GFP (control)	101		10	13
ppl>dcr-1^{RNAi},dp53$^{H159.N}$	103	p < 0,0001	7 (-30%)	13 (=)

Table S1. Related to Figures 1, 2, 6, S1, S2 and S4

Table compiling the number of individuals (n), p-values according to the Mantel-cox test, median survival values (in days, or otherwise specified), and maximum survival values (in days, or specified otherwise) corresponding to the different genotypes of all the experiments of survival to nutrient deprivation shown in Figures 1, 2, 6, S1, S2 and S4.. The change (in percentage) with respect to the control values is shown in brackets.

Gene/transcript	CG number	Primer pair used for qRT-PCR
AKH	CG1171	F: ATGAATCCCAAGAGCGAAGTCCTC R: CTACTCGCGGTGCTTGCAGTCCAG
INR	CG18402	F: GCTGTCAAGCAAGCAGTGAA R: TCTTTTTACCCGTCGTCTCC
4EBP	CG8846	F: AACCCTCTACTCCACCACTC R: CAATCTTCAGCGACTTGG
FAS	CG3523	F: CGGAGAAGAGTTACATCCTG R: CAATCACCACCTTTACGC
MDY	CG31991	F: CTCTTTAGTGCATATCTCGCTCTG R: AACAAGCCCAAGCCCTCT
BMM	CG5295	F: TCCCGAGTTTCTGTCCAAGT R: GCGTCCTTTCTGTGCTTCTT
CG5966 (lipase)	CG5966	F: CTCGCAGTGTCCTTTCCTTG R: TGCTCCTGGTAATCCTCCTG
LPIN	CG8709	F: CTCGGCGGCTATCAAAAA R: ACCTTGTCGTTGTGCTTCCA
UGP	CG4347	F: AACAACATTTGGGCCAACC R: TCCATGTTTAAGGTACGCTCAC
PYK	CG7070	F: CGAACAGATCGCCGGACGCA R: TGACAGTAAAGGTGAACTCGCGG
PGM	CG5165	F: AACTGGCTCCAATCACATCC R: AGCGCACTCCTCATAATCGT

Gene/transcript	CG number	Primer pair used for qRT-PCR
HEX-C	CG8094	F: CACTGGCACCTTGATGTCCT R: GTCCAACTGACCACCCTCAC
TRE T1	CG30035	F: TTGAGGTCACCCAAGATGCT R: AAGGGTCCTCCGGCTATG
GLU T1	CG43946	F: TCTCGGATTCGTCGTCTTCT R: TGAACGGCAAGAACGTGTAG
PDH	CG7010	F: GCAAGGGCGTCAATCACTAA R: TTCTACGGGGTTCTCATCGT
ACOT	CG4581	F: GAAGAACAGCCAGAATATCG R: CACGATGTAGTCGATGAGC
SCOX	CG8885	F: CTCCCGCAGATTCCACTAAA R: TCCTTCATTCTCGCCTCATC
GLS	CG42708	F: CGAGACGGGTTCTTCGGCGG R: CGTGCAGATGCTCAGGCCCC
DCR-1	CG4792	F: CATTGCGTTCACCTCCAAG R: TACTGCCGCTCGTTAGCATT
DROSHA	CG8730	F: TTTCACCCACTTGACCCTTG R: ATTCCCAAATCATCGCAAAC
AGO1	CG6671	F: ATGGAAACCGAACCAAACCT R: GCGGCAGATACCCTATGATG
PRI-MIR-305	CR43032	F: ATCAGGTGCTCTGGTGTGTCT R: CTTGTATCGGTCGCTTTCGT

Table S2. Related to Figures 1, 5 and S1

Table compiling the list of primers used for expression analyses and the corresponding gene names and CG numbers.

Supplemental Experimental Procedures

Drosophila stocks

dp53^{ns}; *dp53^{5A14}*; *UAS-dp53$^{H159.N}$; UAS-dp53$^{2.1}$; UAS-TOR^{TED}* [a truncated version of TOR that dominantly suppresses dTOR activity**,** (Hennig and Neufeld, 2002)]; *UAS-Rheb*; *UAS-GFP*; *UAS-myrTomato*; *hh-gal4*; *cg-gal4*; *Df(2L)exel7031* (*Df(miR-305)* in the text, a deficiency of 130 kbp that covers the *miR-305* locus) were from the Bloomington Stock Center and are described in Flybase. *UAS-dp53^{RNAi}* (v38235); *UAS-dicer^{RNAi}* (v11429) were from the Vienna Drosophila RNAi Center (VDRC). *dcr-1^{Q1147X}* (Hatfield et al., 2005); *actin>CD2>GAL4* (Pignoni and Zipursky, 1997); *UAS-miR305* (gift from Norbert Perrimon); *UAS-Slif^{anti}* and *ppl-gal4* [gift from J. Colombani and P. Leopold, (Colombani et al., 2003)]; *yolk-gal4* (gift from JM Reichhard); *mef2-gal4* [gift from N. Perrimon, (Demontis and Perrimon, 2010)]; *Dp53R-GFPnls* (gift from John M. Abrams, (Lu et al., 2010)), a*p^{Gal4}* (Milan and Cohen, 1999) and other stocks are also described in Flybase. *ppl-Gal4* and *cg-Gal4* are expressed in non-fat-body-related tissues, but their expression domains intersect only in the fat body (Geminard et al., 2009). *yolk-gal4* is expressed only in fat body cells of adult females (JM Reichhard, personal communication to Flybase). In all the presented experiments, all drivers produced identical results, ensuring that the effects are due to fat-body expression. Expression levels of the three GAL4 drivers, monitored by the expression of an UAS-GFP transgene, was mildly reduced upon starvation, most probably as a consequence of the decrease in whole-animal metabolism (Figure S2). Since all experimental conditions were compared with control flies expressing GFP under the same FB-gal4 driver, these changes might not explain the reduced survival rates or accelerated consumption of energy resources observed in FB>Dp53-DN and FB>Dp53-RNAi flies.

Mosaic analysis

The following genotypes were used to generate loss-of-function clones by the FLP/FRT technique (Xu and Rubin, 1993):

hs-FLP/+; GFP-dp53-sensor/+; FRT82 dcr-1^{Q1147X}/FRT82 arm-lacZ

hs-FLP/+; GFP-dp53Δ305-sensor/+; FRT82 dcr-1^{Q1147X}/FRT82 arm-lacZ

hs-FLP/+; Df(2L)exel7031 FRT40 / arm-lacZ FRT40; GFP-dp53-sensor/+

hs-FLP/+; Df(2L)exel7031 FRT40 / arm-lacZ FRT40; GFP-dp53Δ305-sensor/+

Heat-shock was induced 3 or 4 days after egg laying (AEL) and late third instar wing discs were dissected. Mutant cells were marked by the absence of β-gal.

The following genotypes were used to induce the expression of various transgenes in single FB cells:

hs-FLP/+; GFP-dp53-sensor/UAS-dcr-1^{RNAi}; actin>CD2>GAL4, UAS-RFP/+

hs-FLP/+; GFP-dp53-sensor/UAS-miR-305; actin>CD2>GAL4, UAS-RFP/+

hs-FLP/+; GFP-dp53-sensor/UAS-TOR^{TED}; actin>CD2>GAL4, UAS-RFP/+

hs-FLP/+; GFP-dp53Δ305-sensor /UAS-TOR^{TED}; actin>CD2>GAL4, UAS-RFP/+

hs-FLP/+; GFP-dp53-sensor/UAS-slif^{Anti}; actin>CD2>GAL4, UAS-RFP/+

hs-FLP/+; GFP-dp53-sensor/UAS-Rheb; actin>CD2>GAL4, UAS-RFP/+

hs-FLP/+; actin>CD2>GAL4, UAS-GFP/UAS-dp53$^{H159.N}$

hs-FLP/+; actin>CD2>GAL4, UAS-GFP/UAS-dp53^{RNAi}

Heat-shock was induced 36 h AEL and 60-72 h later (including the starvation treatments) were dissected (except for UAS-TOR^{TED} and UAS-slif^{Anti}, which were induced 60 h AEL and dissected 24 h later). Clones were marked by the expression of RFP or GFP.

Antibodies

Rat anti-dILP2 (Geminard et al., 2009); rabbit anti-GFP (Invitrogen); mouse anti-GFP (Roche); rabbit anti β-gal (Cappel); rabbit anti-Gal4 (Santa Cruz Biotechnology). Secondary antibodies were obtained from Molecular Probes.

Constructs

In order to generate the dp53-3’ UTR sensor, the dp53-3′ UTR was amplified by PCR from the GH11591 plasmid (DGRC) and cloned into the control-sensor plasmid (P-CaSper4-tub-EGFP, (Brennecke et al., 2003)) via the NotI-XhoI cloning sites. The following primers were used: forward, 5’-CTTCTGATCTGGTCGACAATC-3’; reverse, 5’-TTTGCAAAATATGACAACTCT-3’.

In order to generate the dp53-3'UTR□305 sensor, the seed region of miR-305 (GTACAAA) on the dp53 3′ UTR was deleted by PCR. The following primers were used to generate the internal deletion: 5'-AACATACTCTAAAGCCAAAAGTGAA-3'; 5'- TTGGCTTTAGAGTATGTTTGTTG-3'.

Multiple transgenic lines were generated per construct.

To generate a dp53-luciferase reporter, the 3'UTR of dp53 was cloned downstream of the pJ-Luc reporter plasmid (gift from E. Izaurralde) via the XhoI-Xba cloning sites. A plasmid expressing Renilla luciferase (RLuc) was used as a transfection control. The 10 candidate miRNAs were amplified by PCR from genomic DNA and cloned into the pAC5.1 plasmid (Invitrogen) via the NotI-Xba cloning sites.

Transfection and luciferase assays

For luciferase assays, S2 cells were co-transfected with the dp53-luciferase reporter, the RLuc transfection control and the corresponding pAc5.1-miRNAs over-expression plasmid, or with the empty vector (pAC5.1) as a control. Luciferase assays were performed 24 h after transfection following the manufacturer's instructions (Dual-Glo Luciferase Assay System, Promega). For each experiment, transfections were performed in duplicates. A representative experiment from three independent replicates was shown.

Quantification of GFP intensity levels in wing discs

Wing discs were imaged using a Leica SP2 confocal microscope. Due to sample thickness, images from 7 focal planes were considered for the determination of mean intensity. The settings on the confocal microscope and all subsequent treatments of images were identical between control and experimental samples. For GFP intensity quantification, the wing pouch of each disc was selected, and mean fluorescence intensity was calculated using Fiji software (NIH). Data were normalized respect to control animals (standard food). Student's *t*-test analysis was carried out for statistical significance.

Fluorescence quantification in IPCs and FB cells

For fluorescence quantification the correspondence tissues from starved or well-fed larvae were imaged using a Leica SP2 confocal microscope. Confocal Z series were taken as described below and identical

microscope settings and all subsequent treatments of images were used between control and experimental samples. Mean fluorescence intensity of average Z-projections was measured using Fiji software (NIH) and data were normalized with respect to *control* animals. Student's *t*-test analysis was carried out for statistical significance. To quantify GFP intensity levels of fat body cells, confocal sections covering the entire nuclei were taken from 10 FBs and a total of at least 100 nuclei per genotype and condition were analysed. To quantify Dilp2 intensity levels in larval brains, confocal sections covering the IPCs were obtained for at least 20 brains per condition.

Nile red staining

The protocol was adapted from (Gronke et al., 2005; Okamura et al., 2007). Briefly, larvae were synchronized in the second to third larval transition and placed in tubes with 2% agar (starved) or standard food (fed) 12 h later. After 24 h, FBs were dissected in PBS, fixed with formaldehyde 4% and stained with Nile red (0.2 μg/ml Nile red) for 30 min. Images were taken on a Leica TCS SP2 confocal microscope.

Starvation treatments

For starvation sensitivity studies in adults, either 1- to 2-days or 5- to 7-days old flies were used. Starvation sensitivity assays were conducted by transferring 15-20 flies of each genotype into vials containing 2% agar and 0%, 1% or 10% sucrose. Flies were transferred to new tubes every day and dead flies were counted every six hours (in experiments of complete starvation with 2% agar and 0%) or daily (in experiments with 1% or 10% sucrose). At least 100 flies per genotype were scored. Starvation sensitivity studies in larvae were adapted from (Palanker et al., 2009). Briefly, eggs were collected for 3 h intervals, and larvae were raised at 25ºC for 48-51 h prior to the starvation assay. Early second instar larvae were washed with water and placed in an inverted 55mm petri dish with two pieces of Whatman filter and soaked with 1 ml PBS 1X. Each plate was sealed with parafilm and incubated at 25ºC for the duration of the experiment. Animals were scored for viability every six hours, and dead larvae were removed. At least 115 larvae per each genotype were scored. In order to estimate the statistical significance between experimental and control groups, non-parametric methods were used for median

survival values: Kaplan-Meier estimator and Log-rank (Mantel-Cox) test using the Graphpad Prism 4.0 software. For the long-term effect of chronic starvation sensitivity, eggs were collected for 3h interval and larvae were raised on either standard food (*Std food*) or diluted food (*0,2X food*) immediately after eclosion. Survival rates were measured as the percent of individuals entering pupariation or giving rise to adult flies. At least 120 larvae per each genotype were scored. Data were normalized with respect to the standard food values and Student's *t*-test analysis was carried out for statistical significance.

Metabolic Assays (extended version)

Briefly, 5 adult males (5 days old) were quick frozen in liquid nitrogen and homogenized in 200 µl of PBST (PBS, 0.1% Tween 20, for TAG measurements), in PBS (for glycogen measurements) and in Trehalase buffer (TB: 5mM Tris pH 6.6, 137 mM NaCl, 2.7 mM KCl, for trehalose measurements) and immediately incubated at 70ºC for 5 min to inactivate endogenous enzymes. For quantification of sugars in circulation, hemolymph was pooled from 40–45 adult flies to obtain 1 µl for assay. Hemolymph was diluted 1:100 in trehalase buffer and immediately incubated at 70ºC for 5 min to inactivate endogenous enzymes before the assay. For TAG assays, 20 µl of heat-treated homogenate was incubated with 20 µl of Triglyceride Reagent (Sigma, T2449) or PBS for 30 min at 37ºC. Samples were centrifuged, and 30 µl of supernatant was transferred to a 96-well plate. One hundred microliters of Free Glycerol Reagent (Sigma, F6428) was added and incubated for 5 min at 37ºC. Absorbance was measured at 540 nm. TAG was determined by subtracting from the total amount of glycerol present in the sample treated with Triglyceride Reagent the amount of free glycerol in the PBS-treated samples and normalized to protein concentration (BioRad). For glycogen and trehalose measurements, 40 µl of heat-treated homogenate was incubated with or without 1 unit of amiloglucosidase (Sigma, A7420, for glycogen measurements) or with 0.05 units.ml^{-1} of trehalase (Sigma, T8778, for trehalose measurements) for 2 h at 37ºC. Samples were centrifuged, and 30 µl of supernatant was transferred to a 96-well plate. Glucose assay was performed by adding 100 µl of Glucose Reagent (Sigma, GAGO20) and incubated 30 min at 37ºC. Absorbance was assessed at 540 nm. Glycogen amounts were determined by subtracting from the total amount of glucose present in the sample treated with amiloglucosidase the amount of free glucose of untreated samples and normalized to

protein concentration (BioRad). Five replicates for each genotype and condition were performed. Data were normalized with respect to the corresponding levels in control flies.

Supplemental References

Colombani, J., Raisin, S., Pantalacci, S., Radimerski, T., Montagne, J., and Leopold, P. (2003). A nutrient sensor mechanism controls Drosophila growth. Cell *114*, 739-749.

Demontis, F., and Perrimon, N. (2010). FOXO/4E-BP signaling in Drosophila muscles regulates organism-wide proteostasis during aging. Cell *143*, 813-825.

Geminard, C., Rulifson, E.J., and Leopold, P. (2009). Remote control of insulin secretion by fat cells in Drosophila. Cell Metab *10*, 199-207.

Gronke, S., Mildner, A., Fellert, S., Tennagels, N., Petry, S., Muller, G., Jackle, H., and Kuhnlein, R.P. (2005). Brummer lipase is an evolutionary conserved fat storage regulator in Drosophila. Cell Metab *1*, 323-330.

Hatfield, S.D., Shcherbata, H.R., Fischer, K.A., Nakahara, K., Carthew, R.W., and Ruohola-Baker, H. (2005). Stem cell division is regulated by the microRNA pathway. Nature *435*, 974-978.

Hennig, K.M., and Neufeld, T.P. (2002). Inhibition of cellular growth and proliferation by dTOR overexpression in Drosophila. Genesis *34*, 107-110.

Lu, W.J., Chapo, J., Roig, I., and Abrams, J.M. (2010). Meiotic recombination provokes functional activation of the p53 regulatory network. Science *328*, 1278-1281.

Milan, M., and Cohen, S.M. (1999). Notch signaling is not sufficient to define the affinity boundary between dorsal and ventral compartments. Mol Cell *4*, 1073-1078.

Okamura, T., Shimizu, H., Nagao, T., Ueda, R., and Ishii, S. (2007). ATF-2 regulates fat metabolism in Drosophila. Molecular biology of the cell *18*, 1519-1529.

Palanker, L., Tennessen, J.M., Lam, G., and Thummel, C.S. (2009). Drosophila HNF4 regulates lipid mobilization and beta-oxidation. Cell Metab *9*, 228-239.

Pignoni, F., and Zipursky, S.L. (1997). Induction of Drosophila eye development by decapentaplegic. Development *124*, 271-278.

Xu, T., and Rubin, G.M. (1993). Analysis of genetic mosaics in developing and adult *Drosophila* tissues. Development *117*, 1223-1237.